Nanostructure and biomimetics orchestrate mesenchymal stromal cell differentiation: An in vitro bioactivity study on new coatings for orthopedic applications

Nanostructure and biomimetics orchestrate mesenchymal stromal cell differentiation: an *in vitro* bioactivity study on new coatings for orthopaedic applications

Maria Sartori [1*], Gabriela Graziani [2*], Enrico Sassoni [3], Stefania Pagani [1], Marco Boi [2], Maria Cristina Maltarello [4], Nicola Baldini [2,4,5], Milena Fini [1].

[1] IRCCS – Istituto Ortopedico Rizzoli, Surgical Sciences and Technologies Complex Structure, via Barbiano 1/10, 40136, Bologna

[2] IRCCS – Istituto Ortopedico Rizzoli, Laboratory of Nanobiotechnology, via Barbiano 1/10, 40136, Bologna

[3] University of Bologna, Department of Civil, Chemical, Environmental and Materials Engineering, via Terracini 28, 40131, Bologna

[4] IRCCS – Istituto Ortopedico Rizzoli, BST Biomedical Science and Technologies Laboratory, via Barbiano 1/10, 40136, Bologna

[5] University of Bologna, Department of Biomedical and Neuromotor Sciences, Via Massarenti 9, 40128, Bologna

*** Co-first Authors as they equally contributed to this work**

Corresponding Author

Maria Sartori, PhD

Surgical Sciences and Technologies Complex Structure

IRCCS – Istituto Ortopedico Rizzoli,

Via di Barbiano 1/10, 40136, Bologna

Email: maria.sartori@ior.it

Phone: +39 0516366942

ABSTRACT

The choice of the appropriate material having suitable compositional and morphological surface characteristics, is a crucial step in the development of orthopaedic implants. The purpose of this paper is to elucidate, on this regard, the influence of two important hits, i.e., biogenic apatite with bone-like composition and nanostructured morphology, providing the evidence of the efficacy of nanostructured biogenic apatite coatings in favoring adhesion, growth, proliferation, and *in vitro* osteogenic differentiation of human mesenchymal stromal cells (hMSCs) isolated from the bone marrow. The specific features of this coating in terms of topographical and biochemical cues, obtained by Ionized Jet Deposition, are perceived by hMSCs, as suggested by changes in different morphologic parameters as Aspect Ratio or Elongation index, suggesting the impact exerted by the nanostructure on early adhesion events, cytoskeleton organization, and cells fate. In addition, the nanostructured CaP coating sustained the metabolic activity of the cells and facilitated the osteogenic differentiation of MSC by supporting the osteogenesis-related gene expression.

These findings support the use of a combined approach between technological advancement and instructive surfaces, both from the topographical and the biochemical point of view, in order to manufacture smart biomaterials able to respond to different needs of the orthopedic practice.

KEY WORDS: titanium, biogenic apatite, nanostructure, ionized jet deposition, mesenchymal stromal cells

1. INTRODUCTION

Biomaterials in healthcare have been the subject of intense research, to constantly improve their characteristics and performance. This general concept, translated into the orthopedic field, means a continuous research and development of biocompatible, bioactive, osteoconductive, osteoinductive biomaterials also able to bear antibacterial properties, as suggested by these decade research trends [1].

For these reasons, biomaterials no longer represent only the passive support for tissue regeneration, repair or functional restoration, but are “active tools”, where the biointerface interacts with the surrounding microenvironment and is capable to orchestrate precise cellular responses. It is widely demonstrated that the microenvironment can strongly influence cell function and behavior, especially in the presence of a biomaterial, that exerts an action on cells influencing their behavior at different levels, depending on its physical, chemical, topographical and mechanical characteristics.

Among the different biomaterials, metals, and in particular titanium and its alloys, are often preferred in the orthopedic field based on their mechanical and structural features [2]. In particular, osteointegrated prostheses for limb amputations, are subjected to high and multi-axial loads, requiring high mechanical resistance and ductility. Titanium alloys can meet such requirements and are biocompatible, although bioinert. However, over the last decades great efforts and achievements have led to master ~~the~~ surface chemistry as a cue to specifically instruct cell fate, conferring metals an enhanced bioactivity and overcoming their intrinsic limits [3,4]. Moreover, advancements in chemistry, nanotechnology and material science have demonstrated that a pattern of different and combined topographical and mechanical signals, are perceived by the cells that react to them [5]. Macro-, micro- and nano-sized topographical cues stimulate changes at the cellular and tissue level [6] and an increasing number of studies have demonstrated the importance of nanoscale surface topography (variation in x and y distances) and roughness of materials, and their correlation with osteogenic differentiation [7].

Mesenchymal stromal cells (MSCs) are distributed throughout several post-natal tissues and organs. They have multilineage differentiation capabilities and properties [8] and play a role, in association with monocytes/macrophage and other inflammatory cells, in the early phase of healing, as key players in governing the interfacial response to material surfaces and in directing osteointegration [9-12]. In addition, it has been demonstrated that MSCs cross-talk with resident cells through paracrine signaling pathways, stimulate the osteogenic differentiation, migration and proliferation of other MSCs [13-15]. Therefore, when studying the biomaterial properties, a fundamental characteristic that should be taken into consideration is the ability of actively recruiting progenitor cells from the surrounding native tissue and to promote their adhesion and differentiation.

To recruit host cells, coatings may be used, with a special focus on nanostructured films having a composition resembling that of bone. Several techniques have been proposed to obtain these films, mainly through bimimetic mineralization and plasma assisted routes [16, 17]. Although biomimetic mineralization provides excellent results in mimicking the composition of the host bone, plasma-assisted techniques, mostly Magnetron Sputtering, Pulsed Laser Deposition and Matrix Assisted Pulsed Laser Evaporation and Pulsed Electron Deposition, guarantee the finest control over film thickness and surface morphology and the highest industrial scalability [18-24]. In particular, Pulsed Electron Deposition (PED) is a plasma assisted technique that has been recently proposed for the biomedical field to obtain nanostructured ceramic coatings, and is a valid and efficient tool for the deposition of nanostructured coatings starting from a biogenic source. Among the main advantages of PED is the fact that it permits a fine conservation of stoichiometry, from the material to be deposited (target) to the coated substrate, avoiding formation of decomposition phases and preferential sputtering, that are common in other plasma-assisted techniques [25-27]. This has been demonstrated also for complex materials, such as ion-subtitued hydroxyapatites and bioactive glasses [28,29]. Regarding the deposition of biogenic sources (bovine bone) by PED, in the Ionized Jet Deposition (IJD) setup, a preliminary study on a reference substrate (borosilicate glass) has been published by the Authors for dental application. Adhesion, proliferation, and osteogenic differentiation of human dental pulp stem cells (hDPSCs) has been evaluated for bone apatite coatings in comparison to stoichiometric hydroxyapatite. This study has demonstrated the biocompatibility of coatings deposited with IJD and their ability to promote the proliferation of hDPSCs and a positive effects in terms of osteogenic commitment [30]. Subsequently, coatings have been applied also to titanium alloys. The composition and morphology of the substrate, including its surface finishing, strongly influence the characteristics of the coatings, in terms of morphology (thickness and nanostructuration) and, possibly, composition. A detailed characterization of the nanostructured coating properties from a compositional, micro-structural, morphological and mechanical point of view has been performed and the optimal deposition and post deposition conditions have been determined [28].

Here, the coatings are proposed for an orthopaedic application, i.e., to increase the integration of osseointegrated prostheses for limb amputation. Therefore, this study aims to combine elements hitherto studied in a separate manner and to provide evidence of the efficacy of the nanostructured biogenic apatite coating deposited on a titanium substrate to favor adhesion, growth, proliferation and differentiation of bone marrow osteogenic precursors.

2. MATERIALS AND METHODS

2.1. Materials

For the bioactivity study, titanium alloy (Ti_6Al_4V) cylinders (∅ 0.5 cm x 0.5 cm) provided by Zare Srl (RE - Italy) and obtained by Selective Laser Melting technique with a final roughness (R_a) of 5 µm were used as a substrate for the deposition. Uncoated cylinders of the same dimensions were used as micro-rough control substrates (referred to as **CTRTi** in the text). Surface roughness was specifically selected to mimic that normally found in orthopedic implants. Coated and uncoated cylinders were also used for all morphological and compositional characterizations and for the dissolution tests. Instead, mechanical tests were performed onto titanium alloy slabs (3 cm x 3 cm x 0.5 cm), having the same composition and surface finishing of the cylinders. Nanostructured biogenic apatite coatings (referred to as **BA** in the text) were obtained by IJD technology, by deposition of biogenic apatite targets. Briefly, biogenic apatite was obtained by deproteinized bovine cortical shafts, shaped into disks (diameter 3 cm, height 0.5 cm) suitable for deposition. Deproteinization was obtained by immersion in a 2.7 wt.% NaOCl solution in deionized water for 14 days under continuous stirring. Efficacy of deproteinization was verified by FT-IR (data not reported).

2.2. Biogenic apatite nanocoating deposition

Biogenic apatite films were manufactured by Pulsed Electron Deposition in the Ionized Jet Deposition (IJD) setup (Noivion Srl, Rovereto, Italy), starting from the deproteinized bone targets. Deposition parameters were selected based on preliminary results aimed at optimizing coating thickness, morphology and adhesion to the substrate [28,30]. Based on these results, the working voltage and the electron beam frequency were set at 17 kV and 7 Hz, respectively, and a 30 minutes deposition duration was chosen, to obtain a thickness of 450±20 nm [28]. After deposition, all films were annealed for 1 h at 400°C in air, to optimize crystallinity.

At the end of the deposition process, and prior to the use in cell cultures, all the substrates were extensively cleaned with several immersion in a graded series of ethanol until a final wash in sterile physiological solution prior to be sterilized with UV light exposition.

2.3. Biogenic apatite nanocoating characterization

Coatings morphology was analyzed by Field Emission Gun Scanning Electron Microscopy (FEG-SEM, Tescan Mira3, CZ, working distance = 10 mm, voltage = 10 kV). Prior to FEG-SEM observation, samples were made conductive by sputtering with aluminum, to avoid charging and interference with EDS detection of Phosphorous. Based on FEG-SEM images (magnification 20,000x and 50,000x), the dimension of the grains that constitute the coatings and their clustering was measured by ImageJ software (National Institutes of Health, USA). To this aim, 3 non overlapping areas

having the same dimension were selected from two samples, each composed by at least 45 clearly distinguishable aggregates. Maximum (Dmax), minimum (Dmin) and most frequent diameter (Df) were calculated: Dmax and Dmin were derived from images at 50,000x magnification, Df from images at at 20,000x.

Films composition was studied by Energy Dispersive X-ray Spectroscopy (EDS). Three non-overlapping regions of two different samples were examined, 2 closes to the samples center and one next to their edges, as for SEM. The EDS analysis was performed using a Bruker probe coupled with a field emission gun scanning electron microscope (FEG-SEM, Tescan Mira3), using a working voltage of 10 kV, on samples sputtered with aluminum. For each area, both elemental spectra and maps were acquired to investigate the amount of trace ions sodium and magnesium (wt.%) and to study the distribution of elements in the coating (Ca, P, Mg, Na), which describes the uniformity in composition.

Composition of the targets and the coatings was also assessed by FT-IR microscopy (Perkin Elmer Spotlight i2000) and X-rays Diffractometry (XRD, Panalytical X'Pert PRO, grazing incidence mode). FT-IR acquisitions were carried out in reflectance mode (resolution of 4 cm^{-1}, 16 scans and data interval 1 cm^{-1}), selecting 6 random non overlapping regions (100x100 μm^2), from 2 samples. XRD patterns (angle $\omega = 2°$, $\varphi = 180°$, scan step size 0.0167, time per step 250.190) were collected in a range $2\theta = 3–15°$ and 20–34° to investigate the areas relevant for calcium phosphates while excluding the peaks of titanium. XRD peaks of stoichiometric and bovine bone apatite powders were also collected, for comparison sake (XRD, X'Pert PRO, Malvern Panalytical, Malvern, UK, φ = 5°–80°, scan step size 0.017°, time per step 50 s).

To evaluate the adhesion of the films to titanium substrates, micro-scratch test was performed according to the Standard ISO 20502:2005, by using a Micro-Scratch Tester (MST, CSM Instruments — Anton Paar S.r.l, Peseux, Switzerland). A conical Rockwell C stylus with a spherical apex indenter tip (angle 120° and sphere radius 100 μm) was used for the acquisition. The load, progressively increasing from 0.01 to 10 N (loading rate 10 N/min), was applied perpendicularly to the surface, with an indenter traverse speed of 10 mm/min. As recommended by the standard, the rate of increase of normal force and the indenter traverse speed were selected based on the critical value of normal force which is forecast for the failure event of interest, which is expected to lower than 10 N [28]. 6 scratch tests were performed on 2 coated samples (3x3x0.5 mm^3 titanium alloy slabs) and the worn tracks of each scratch were examined. Failure modes of the coating were assed and associated to the value of the critical normal load at which they occurr (Lcn).

Coatings stability was evaluated by SEM/EDS, after immersion in sterile alpha-MEM (Minimum Essential Medium Eagle, Sigma Aldrich) supplemented with 1 wt% penicillin-streptomycin (to avoid bacterial contamination). Medium pH was adjusted to 7.4 by addition of $NaHCO_3$ (2.2 g/l). Coated plates (2 per timepoint) were placed inside 24 wells in 1 ml medium and incubated for 1 day, 7 days and 14 days. 14 days exposure was selected as it is the timepoint used for *in vitro* tests. Medium was refreshed every 72 hours. Well plates were kept sealed in a humidified incubator at 37 °C,

95% air and 5% CO_2 for the whole duration of the tests. Progressive dissolution of the film was studied by comparing the morphology of the coating at different time points (acquisition by FEG-SEM, processing by ImageJ). EDS was also used to confirm the presence of Ca and P at each timepoint, which are characteristic of the presence of the coating. FEG-SEM/EDS was performed as described as above on at least 2 non-overlapping areas for each sample, Specific attention was devoted to the coating integrity at each timepoint and to the presence/absence of cracks and detachments, which are considered detrimental, as they could result into inflammation and toxicity upon implantation in vivo.

2.4. Cell culture

Human bone marrow-derived mesenchymal stromal cells (hMSCs) were purchased from ATCC® (batch PCS-500-012™). Cells were thawed and plated in 75 cm^2 tissue culture flasks with standard culture medium (*MesenCult Human MSC Basal Medium* - STEMCELL Technologies Inc). The culture medium was refreshed every 2 days and adherent hMSCs were cultured until 80% confluence in a humidified atmosphere, 5% CO_2 at 37 °C. Cells were detached using tripsin/EDTA (Sigma Aldrich, Missouri, USA) for 5 min and counted in a Neubauer chamber using Erythrosin B exclusion dye (Thermo Fisher, Kandel, Germany). Human MSCs were used at passage 4.

2.5. Cell seeding

Human MSCs suspension of 10 µl was seeded dropwise onto BA and CTRTi substrate. A seeding density of 5,000 cells/cm^2 for substrate was adopted for adhesion, cell morphology evaluation and SEM analyses, while a cell seeding density of 10,000 cells/cm^2 was used for metabolic activity evaluation and gene expression.

After seeding, hMSCs were left on the substrates for 1 h at 37 °C without medium to allow cells adhesion. Then, standard culture medium was added to completely cover the substrates. Twenty-four hours after seeding, samples were removed from the original wells and placed in a new plate and the following experimental conditions were settled up:

- CTRTi cultured in osteogenic differentiation medium (*StemPro™Osteogenesis Differentiation Kit*) (referred to as **CTRTi_OSTEO** condition in the text);
- BA in osteogenic differentiation medium (referred to as **BA_OSTEO** condition in the text);
- BA in standard culture medium (referred to as **BA_nDIFF** condition in the text);
- Human MSCs seeded onto polysterene and cultured in the osteogenic medium (referred to as **CTRcells_OSTEO),** adopted as control of the osteogenic differentiation of hMSC and cells cultured in standard medium (referred to as **CTRcells_nDIFF)** adopted as control of the culture itself. These two conditions represent a 2D control of the culture, as reported in the literature, that indicate hMSCs cultured in tissue culture polystyrene, as the optimal reference material for *in vitro* characterizations [31].

The cultures were kept at 37 °C in a 5% CO_2 humidified atmosphere for 3, 7 and 14 days.

2.6. Early cell adhesion

Early adhesion and morphological features of hMSCs onto the BA and CTRTi substrates were visualized by staining the cells at 2, 4 and 24 hours of culture. The substrates were washed with Phosphate Buffered Solution (PBS), fixed with a cold solution of 4% paraformaldehyde in PBS for 30 min, permeabilized with 0.5% Triton X-100 for 10 min and blocked with a solution containing 1% of bovine serum albumin (BSA) in PBS for 30 min. This step was followed by the incubation with a mouse anti-vinculin antibody (Sigma, code: V9131, dilution 1:350 in PBS-BSA 0.1%) for 2 hours at room temperature in the dark. Afterwards, substrates were incubated with a goat anti-mouse antibody coupled with AlexaFluor 568, (Invitrogen, code: A-11004) diluted 1:500 in PBS 1% at room temperature for 30 min. To visualize the actin filaments of cytoskeleton, another incubation with FITC-conjugate phalloidin solution (50μg/ml) in PBS was performed for 45 min at 37°C. In the final labelling step, substrates were incubated with the specific nuclear dye DAPI solution (2 μg/ml) for 10 min in the dark and washed twice with PBS. Substrates were stored at 4 °C before fluorescence imaging capture. After each incubation step, successive washes with PBS were performed. The staining's were visualized using an inverted microscope equipped with an epifluorescence setup (Eclipse TiU, NIKON Europe BV, NITAL SpA, Milano, Italy). Different fields were acquired for each substrate at 20x and 40x magnification. Inside each field, individual cells were manually outlined using Cell^B software (Olympus) to perform morphometric measures. Area, perimeter, circularity, roundness, aspect ratio and elongation index) were quantified for at least 30 cells per substrate employing ImageJ software (Version 1.53c, National Institutes of Health, Bethesda, MD, USA). Circularity was calculated as [(4π(cell area)/(cell perimeter)], Elongation index was defined as [(cell perimeter)2/(4π(cell area))], aspect ratio was calculated as major axis/minor axis, while roundness was defined as [(4cell area)/(π(major axis)2)].

The study of focal adhesion points (FA) was performed onto the images acquired at 40x. To quantify the focal adhesion points, fluorescence images of vinculin staining were converted with ImageJ to an 8-bit file, and the background was subtracted. Then, a threshold was adjusted to detect focal adhesion points number and area using analyze particles function. The number of focal points was counted per cell and normalized by the cell area and expressed as FA/μm2.

2.7. Scanning electron microscopy

Mesenchymal stem cells seeded onto substrates were also processed for Scanning Electron Microscopy (SEM) (n=3). At 3, 7 and 14 days substrates were fixed in 2.5% glutaraldehyde, in pH 7.4 phosphate buffer 0.1M for 1 hour and subsequently dehydrated in a graded ethanol series (30-50-70-95%) for 10 min each and ethanol 100% for 1 hour. After

two consecutive passage in hexamethyldisilazane (5 minutes each) the samples were left to dry overnight. A thin gold layer was sputtered onto all samples before image acquisition ~~with~~ by Scanning Electron Microscope EVO/MA 10 Zeiss.

2.8. Cell metabolic activity

To test cell metabolic activity, Alamar blue dye (Serotec, Oxford, UK) was added to experimental and control cultures (1:10 v/v) at 3, 7 and 14 days, according to the manufacturer's instruction. Alamar Blue assay is based on the use of resazurin, a water-soluble, stable non-toxic and permeable through cell membranes reagent that allows the monitoring of the reducing environment of the living cell. The reagent was incubated for 4 hours at 37°C and during the test the viable cells with active metabolism reduced the reagent resazurin into the resorufin in the mitochondria of the living cells. The quantity of resorufin produced is proportional to the number of viable cells, thus representing a viability assay [32]. The absorbance of resorufin was read at 570 e 600 nm wavelenghts by a Micro Plate reader (Bio-Rad Laboratories,CA) and the obtained values were converted to a percentage of reduction of the Alamar Blue reagent by using the molar extinction coefficients of the oxidized and reduced forms of the reagent:

$$\% \text{ of reduction} = (O2 \times A1) - (O1 \times A2) \;/\; (R1 \times N2) - (R2 \times N1) \times 100$$

where:

A1 = Abs at 570 nm
A2 = Abs at 600 nm
O1 = 80586 = Molar extinction coefficient of the reagent in oxidized form at 570 nm
O2 = 117213= Molar extinction coefficient of the reagent in oxidized form at 600 nm
R1 = 155677= Molar extinction coefficient of the reagent in reduced form at 570 nm
R2 = 14652 = Molar extinction coefficient of the reagent in reduced form at 600 nm
N1 = Abs of the negative control (medium/Alamar, w/o cells) at 570 nm
N2 = Abs of the negative control (medium/Alamar, w/o cells) at 600 nm

2.9. Gene expression

Total RNA was extracted from BA_OSTEO, BA_nDIFF, CTRTi_OSTEO, CTRcells_nDIFF and CTRcells_OSTEO by PureLink ™ RNA Mini Kit (Ambion LifeTechnologies Lot 1762392), quantified by a NANODROP spectrophotometer (NANODROP 2720, Thermal Cycler, Applied Biosystem) and reverse transcribed with the Superscript VILO cDNA Synthesis kit (Life Technologies), according to the manufacturer's instructions. Each sample was diluted up to a final concentration of 5 ng/µl, taking into account the amount of extracted RNA.

Gene expression was evaluated by semi-quantitative PCR analysis using the SYBR Green PCR kit (Qiagen) in a Light Cycler 2.0 instrument (Roche Diagnostics). Five nanograms of each sample were tested in duplicate, in capillaries. The protocol included a denaturation cycle at 95 °C for 15 min, 40 cycles of amplification (95 °C for 15", appropriate

annealing temperature for each target, as detailed in Table 1, for 20", and 72 °C for 20") and a melting curve analysis to check for amplicon specificity.

The results are obtained by using the mean threshold cycle applied to the $2^{-\Delta Ct}$ method, with GAPDH as reference gene (also referred to as housekeeping gene). In this way the molecules' number of the gene of interest per 100,000 molecules of GAPDH is obtained.

GENE	Primer forward	Primer reverse	Amplicon Lenght	Annealing Temperature
GAPDH	5'TGGTATCGTGGAAGGACTCA3'	5'GCAGGGATGATGTTCTGGA3'	123 bp	56°C
RUNX2	QuantiTect Primer Assay (Qiagen) Hs_RUNX2_1_SG_QT00020517		101 bp	55°C
COL1A1	QuantiTect Primer Assay (Qiagen) Hs_COL1A1_1_SG_QT00037793		118 bp	55°C
ALPL	QuantiTect Primer Assay (Qiagen) Hs_ALPL_1_SG_QT00012957		110 bp	55°C
BGLAP	QuantiTect Primer Assay (Qiagen) Hs_BGLAP_1_SG_QT00232771		90 bp	55°C
SPARC	QuantiTect Primer Assay (Qiagen) Hs_SPARC_1_SG_ QT00018620		60 bp	55°C
BMP2	5'TTTGACCAGAGTTTTTCCATG3'	5'GAAGCAGCAACGCTAGAAGA3'	130 bp	60°C

Table 1: Specifications of primer used for the gene expression analysis.

2.10. **Immunoenzymatic Assays**

At 3, 7 and 14 days Enzyme Linked Immunosorbent assays (ELISA) have been performed to quantitative measure the protein release of some of the main osteogenic markers. The supernatants from each experimental group were harvested, centrifuged to remove particulates and stored at -70°C until the use. Briefly, 100 µl of cell culture supernatant was added to 96 well plates coated with antibody specific to human Alkaline Phosphatase (ALP- Fine Test, Fine Biotech Co, Ltd, Wuhan, China. Catalogue No: EH2618), or Osteocalcin (OC- Fine Test, Fine Biotech Co, Ltd, Wuhan, China. Catalogue No: EH3468) or Collagen Type I (COLL1- BIOMATIK, Biomatik Corporation, Cambridge, Ontario, Canada. Catalogue: EKU03297) and the assays were performed according to manufacturer's instructions. Finally the concentration of the markers was calculated by reading the absorbance at 450 nm on a spectrophotometer (Micro Plate reader - Bio-Rad Laboratories,CA)

2.11. Statistical analysis

The statistical analysis was carried out using the software R v.3.6.1 (*R Core Team (2013)* and the lme4 application packages [33] and emmeans [34]. After verifying the normal distribution of the data by Shapiro-Wilk test and the homogeneity of variance (Levene Test), data were analyzed using linear models.

In detail, for the cell metabolic activity (Alamar Blue test) and morphometry data, a mixed linear model was used for repeated measurements in which the fixed factors were:

- for the cells metabolic activity, the type of substrate (5 levels - BA_OSTEO; BA_nDIFF; CRTI_OSTEO; CTRcells_OSTEO; CTRcells_nDIFF) and the experimental time (3 levels - 3, 7, 14 days);
- for morphometry and focal adhesion points: the type of substrate (2 levels - CTRT and BA) and the experimental time (3 levels - 2, 4 and 24 hours).

The random factor was the experiment (4 levels). A linear model was used for gene expression data (qRT-PCR) and ELISA assays in which the fixed factors were the same used for cell metabolic activity. After evaluating the presence of interaction between the factors or of single effects of the factors on cell metabolic activity, morphometry, gene expression and ELISA data, comparative evaluations were carried out using the marginal means estimated by the models with the correction of the *p* values for the multiple comparisons according to Holm.

3. RESULTS

3.1. Coatings characterization

FT-IR spectra (Figure 1) indicate that all films are composed of carbonated hydroxyapatite, as shown by the bands at 1455, 1402 cm^{-1} (antisymmetrical and symmetrical stretching modes of $CO_3\nu_3$), 867 cm^{-1}(ν_2 CO_3), 1030 cm^{-1} (ν_3 PO_4 antisymmetric stretch), 600 cm^{-1} (ν_4 PO_4 antisymmetric bend). The curves of different samples and different areas perfectly overlap, indicating a very high uniformity in composition between different samples and among different areas within one sample, different from what found for many plasma-assisted deposition techniques where secondary phases are frequently assessed, uniformly or non-uniformly distributed in the coating [25-27].

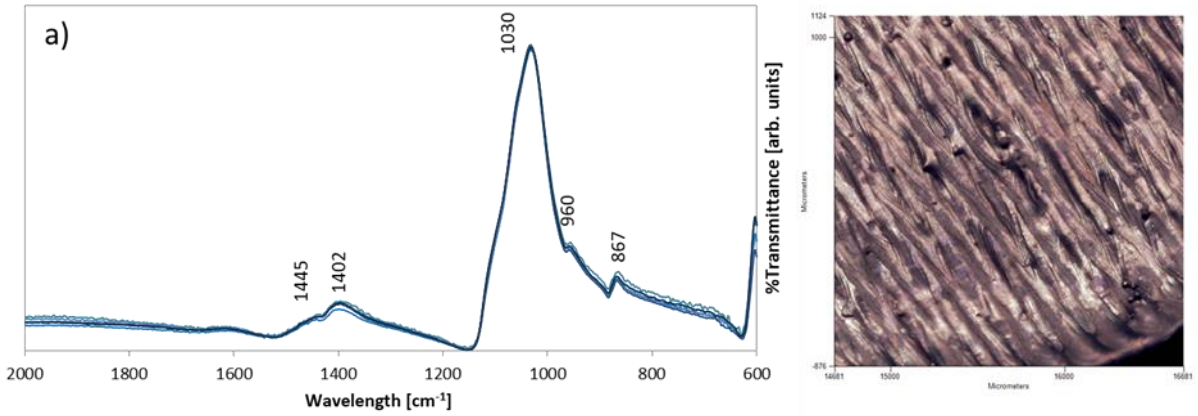

Figure 1. FT-IR spectra acquired in 6 random regions (100x100 μ^2) of 2 samples.

GI-XRD spectra (supplementary material, **Figure S1**) confirm that the coatings are composeed of hydroxyapatite and have a low degree of crystallinity, as a broad peak is noticed in the 30-33° area. As for FT-IR, no secondary phases are detected (metastable CaPs), nor decomposition phases, such as CaO, as no other peaks are visibile in the spectrum, apart from those characteristics of HA. The presence of octacalcium phosphate (OCP, figure S1a) can also be excluded, as no peaks are detected in the $2\vartheta = 3–15°$ area of XRD patterns. Notably, a discrimination among CHA and HA is not possible here, given the low thickness and the low crystallinity of the films, both resulting in a widening and an ill-defined shape of the peaks.

EDS indicates the presence of trace ions sodium (0,11 ± 0,02 wt%) and magnesium (0,47 ± 0,05 wt.%) in a percentage close to that of native bone. EDS maps (Figure 2) indicate a highly uniform distribution of all elements (Ca, P, Mg and Na) in all areas of the coated samples, including those closer to the edges, which are more prone to disomogeineity and defects. Again, the presence of inhomogeneous areas, having a composition different from the bulk coating, is excluded.

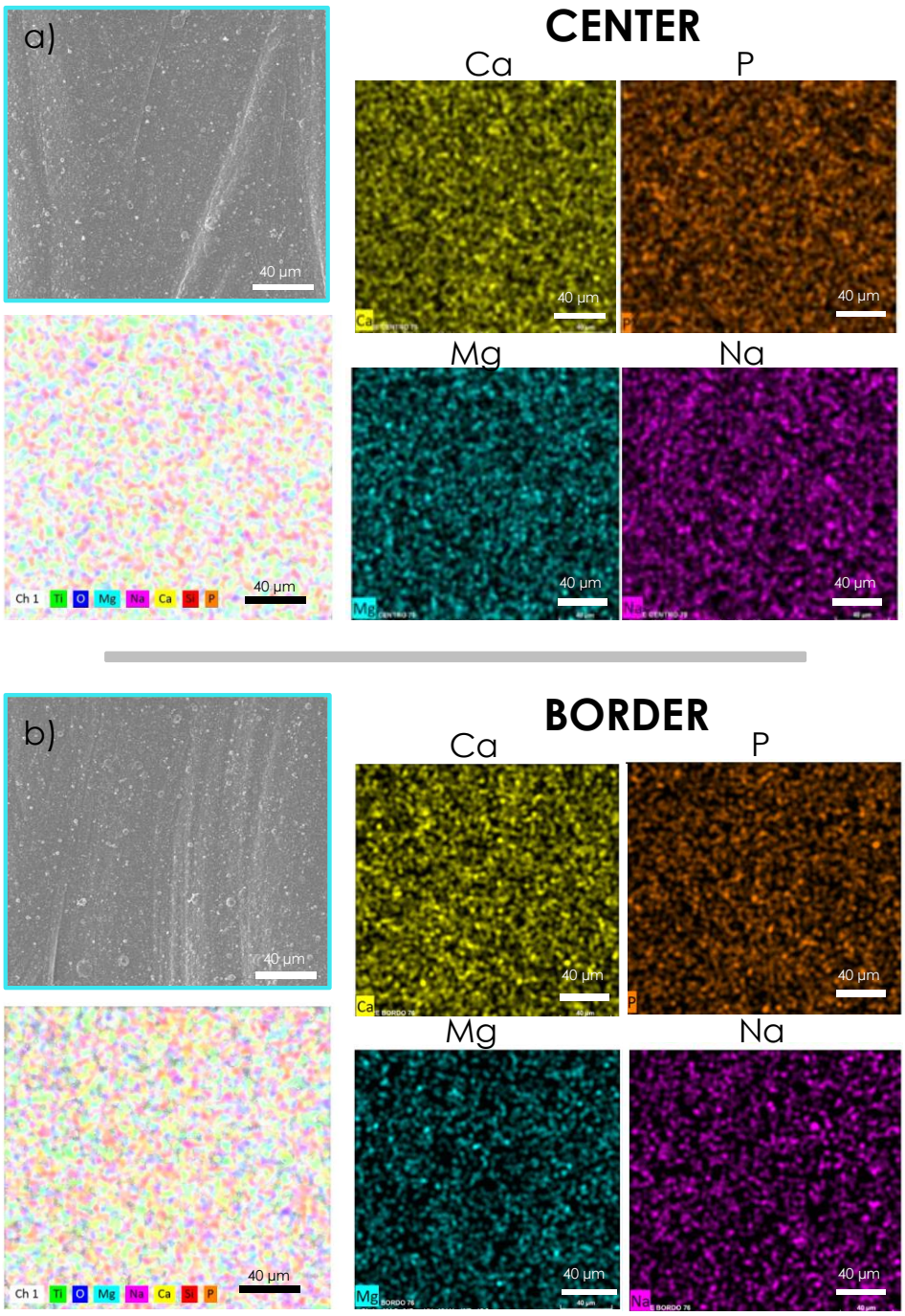

Figure 2. EDS maps acquired in the a) central part of the samples and b) close to the samples edges. Ca, P, Mg and Na are highlighted as they are the main components of the biogenic apatite coatings.

From a morphological point of view, films are composed by nanosized globular aggregates (Figure 3 e, f, h, i). At the macro- and micro-scale, coatings appear homogeneous, as no defects are noticed, nor morphological differences between the different areas of the samples (center vs borders). This indicates that the selected deposition parameters (target-substrate distance, substrate rotation) are effective in mitigating the spatial heterogeneity characteristic of plasma-assisted techniques, which depends on the distance from the plasma plume and its angle of incidence with the

sample surface. Because of the nanoscale thickness of the films, they do not alter the microscale surface finishing of the implants (Figure 3a, b, d, e, g, h), that is designed to guarantee primary stability to the implant.

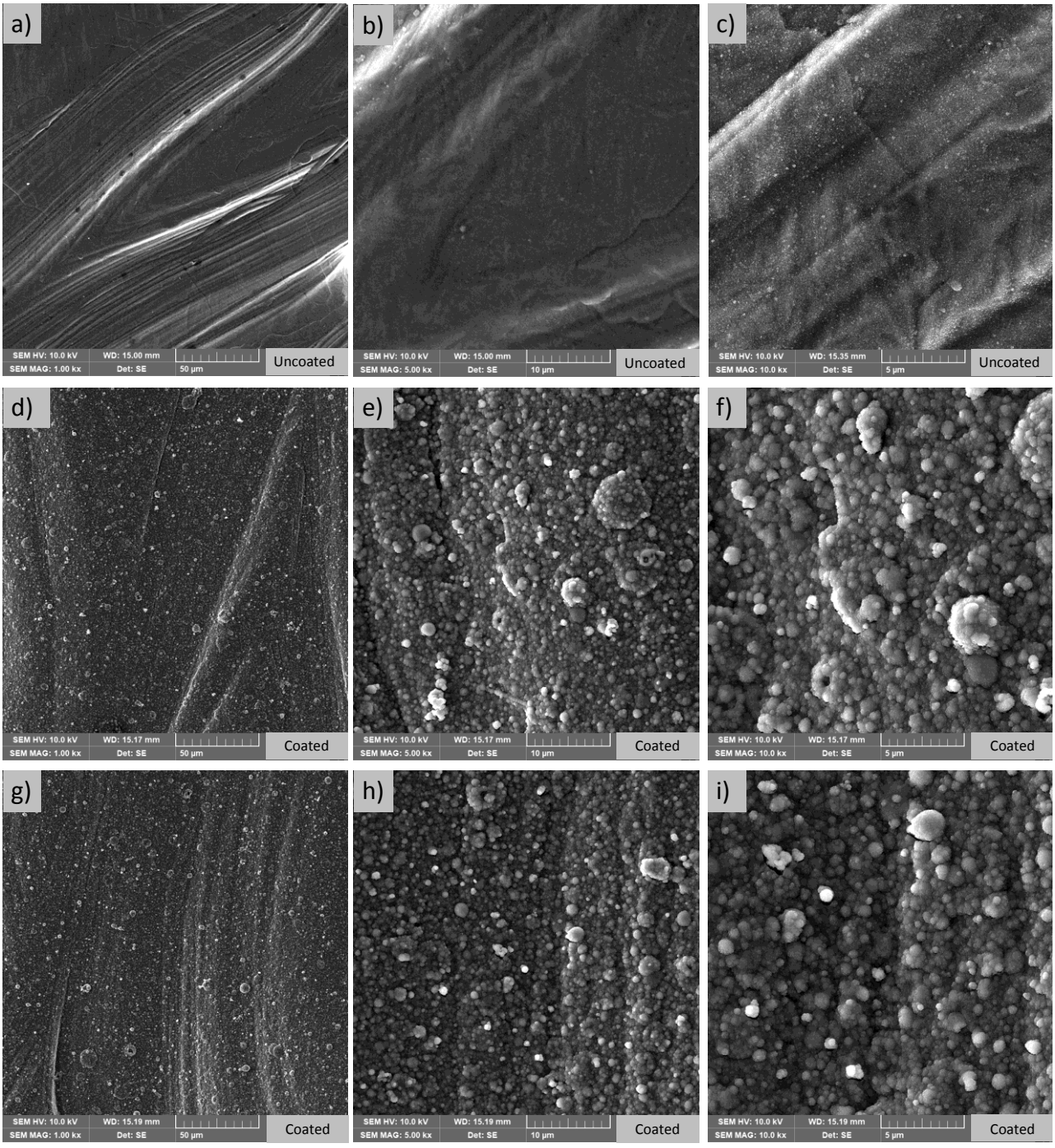

Figure 3. Morphology of uncoated (a-c) and coated (d-i) samples. Morphology is examined in different positions of the samples, including their center (d-f) and the samples borders (g-i).

At higher magnification (Figure 4), it is clear that the coatings have multi-scale features. In fact, they are composed by nanosized grains (diameter ~ 40 nm, Table 2) that tend to aggregate in multi-scale clusters, randomly distributed in the coating. The majority of clusters have a diameter in the range of 100 nm, but they can reach diameters up to about 2

microns. Again, no significant differences are assessed among the samples center and borders, apart from a slight increase in the maximum diameter in the central parts.

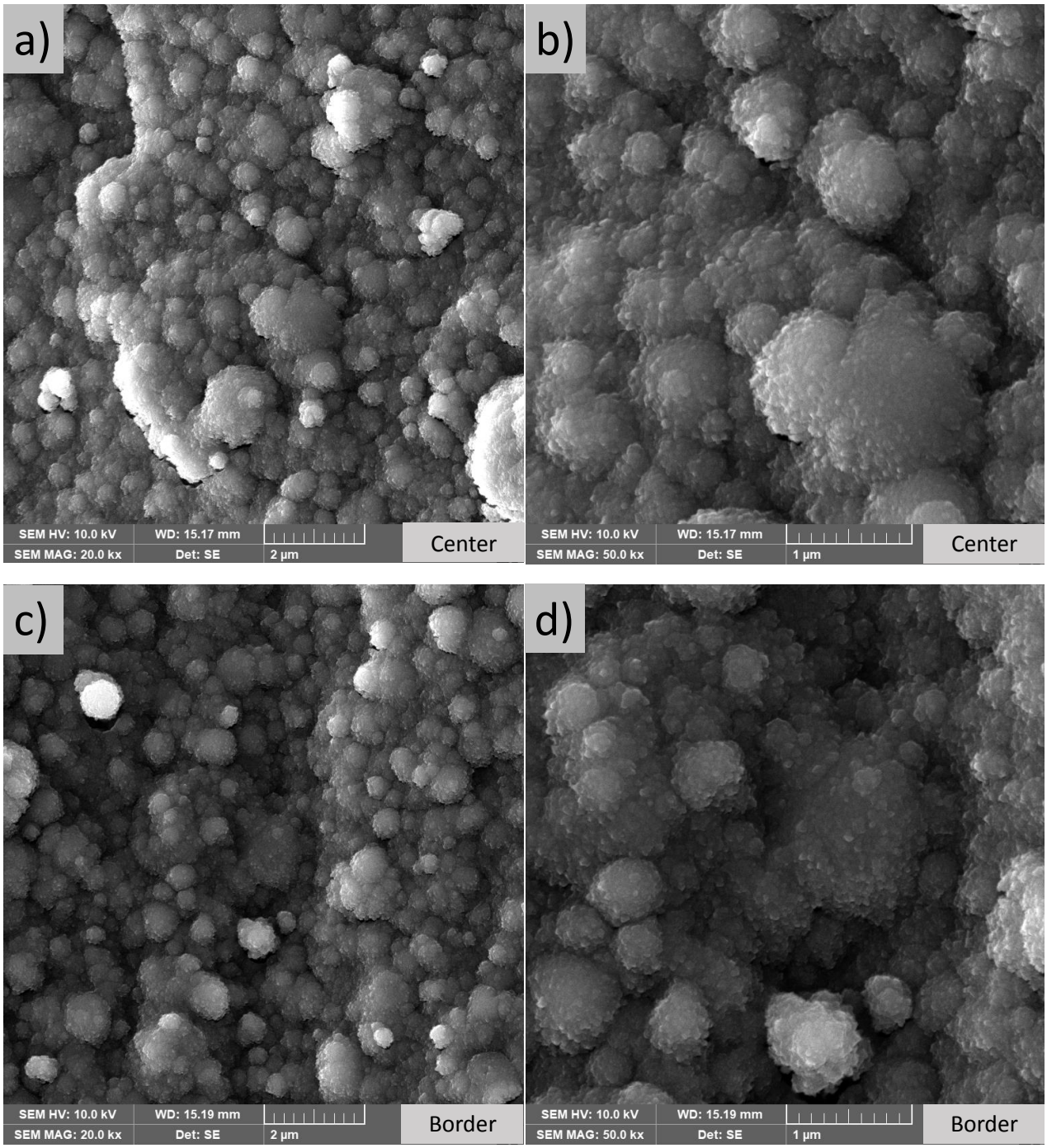

Figure 4. Surface morphology of the films.

	Dmin [nm]	Dmax [nm]	Df [nm]
Center	38	1866	122
Border	37	1776	111

Table 2: Minimum, maximum and most frequent diameter in the nanostructured films

Results of scratch test are reported in Table 3. Values obtained for critical loads are in good agreement with those measured for films deposited by PED and similar techniques, such as PLD (LC2 up to ~2–3 N for films with similar thickness and surface morphology) [28, 35, 36]. All values of critical loads are below 10 N, hence the parameters selected for traverse speed and load increase rate don't need to be adjusted.

LC1 [N]	LC2 [N]	LC3 [N]	LC4 [N]
0,31±0,09	1,44±0,45	6,68±0,85	8,09±0,82

Table 3: Adhesion of the bone apatite films, as measured by micro-scratch test. In the Table, LC are the values of critical failure loads, defined by ISO 20502:2005: LC1 = First cracking; LC2 =Edge chipping; LC3 =First delamination within the track; LC4 =Full delamination or Massive delamination.

Dissolution profile of the coatings, after 1, 7 and 14 days of immersion in alpha-MEM was described in Figure 5. Tests indicate that the films remain substantially unaltered even after 14 days exposition in medium, as the aggregates are cleasly visible at each timepoint. The presence of the coating at each timepoint was also confirmed by EDS (**Figure S2**). No thinning of the films is suggested, as it would results in a progressively increased visibility of the surface finishing on the implant, behind the coated layer [37]. At high magnification (Figure 6), the shape and dimensions of the aggregates and their clustering appear unaltered. This indicates that the coating does not experience too fast a dissolution, that would result into excessive ion release and interfere with cells viability. In addition, no defects are noticed, such as cracking scaling and delamination, apart from some isolate areas in the one of the coating exposed for 7 days (Figure 5d). Because the defects are not assessed at 14 days exposure, they can be ascribed to incorrect handling during the deposition or testing phases. The absence of excessively fast dissolution, fracturing and disomogeneities in dissolution are consistent with the coatings bone-like crystallinity, high adhesion, composition uniformity and absence of decomposition phases, respectively.

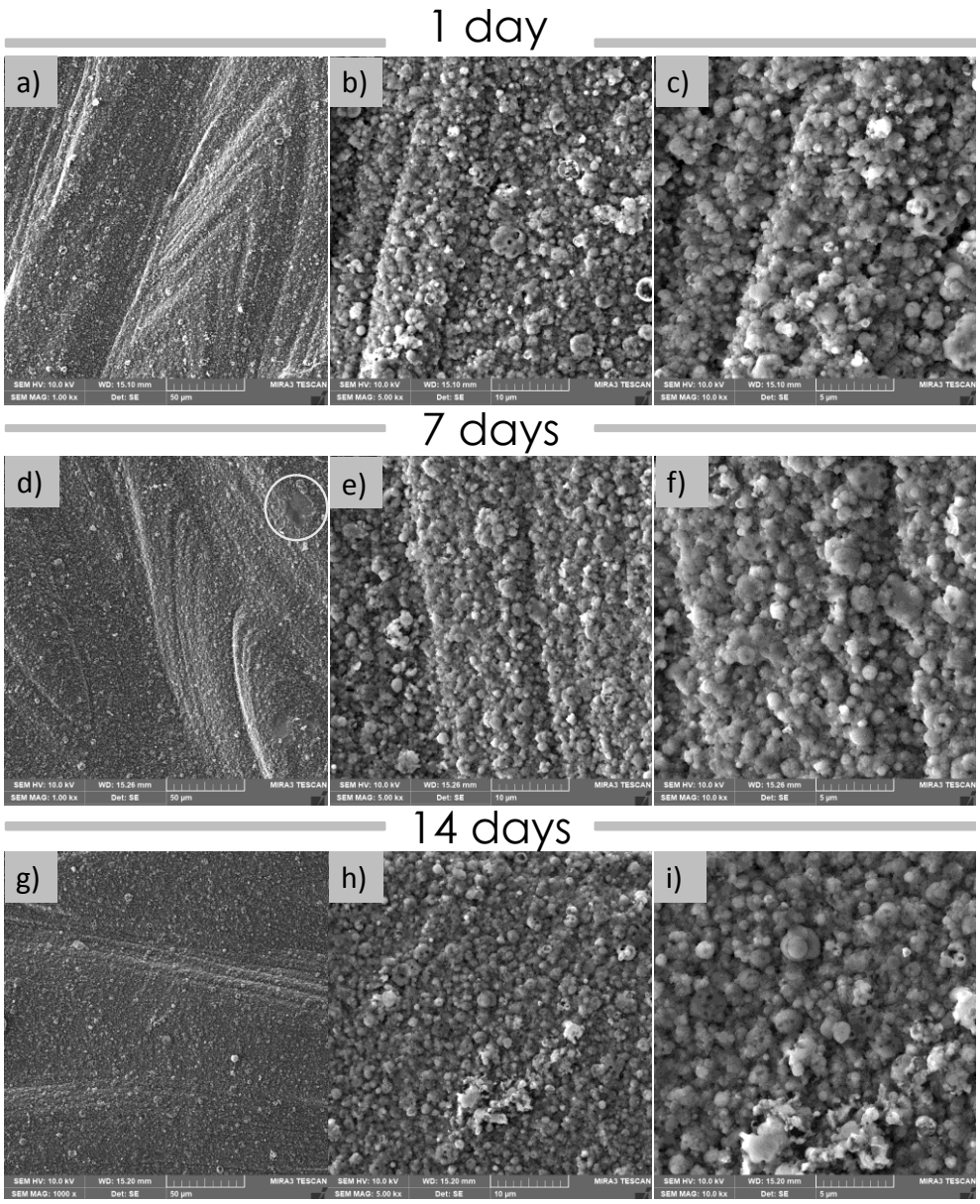

Figure 5: Samples morphology after (a-c) 1 day, (d-f) 7 days and (g-i) 14 days immersion in alpha-MEM. In d) the white circle indicates a defect in the coating

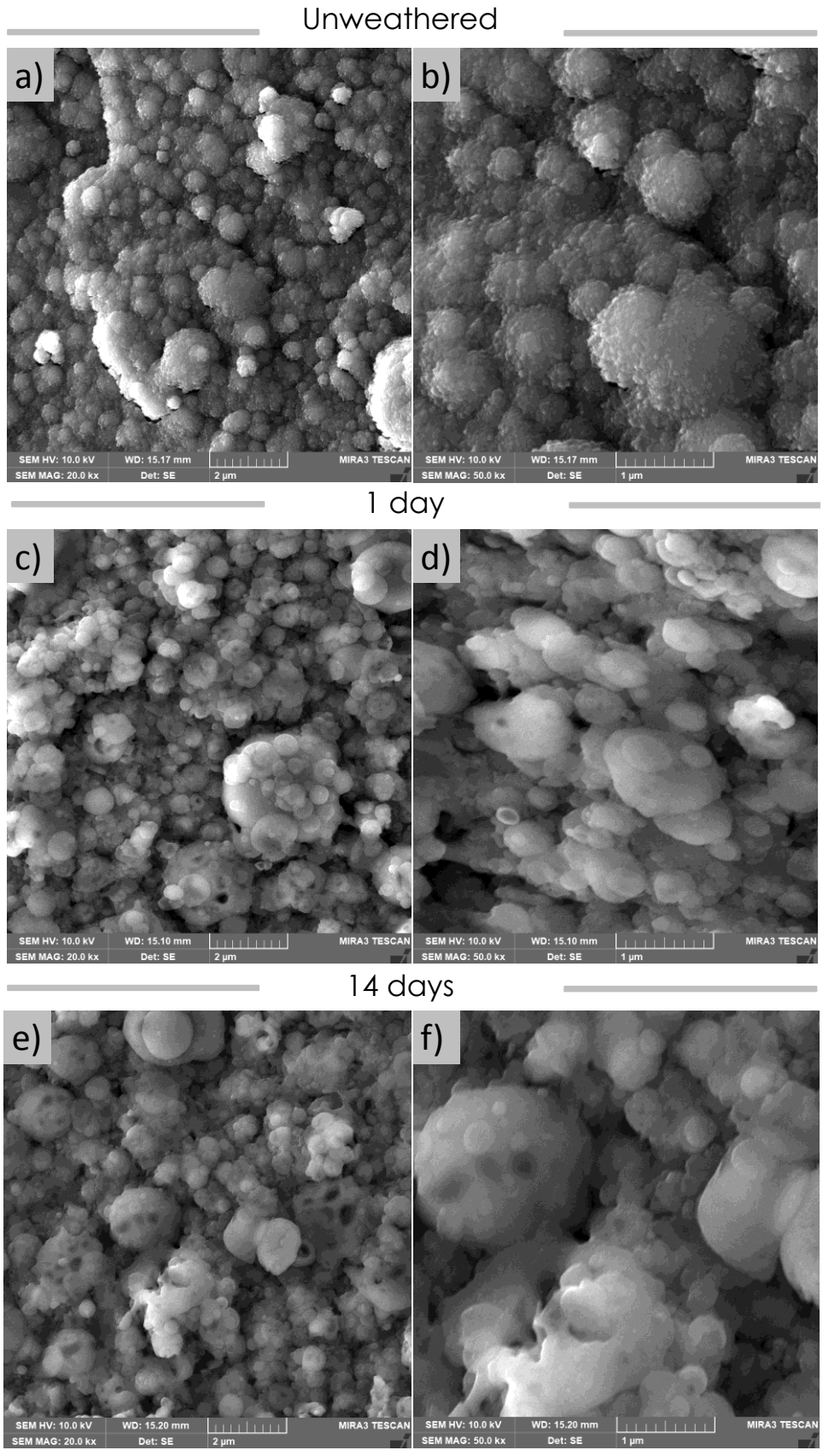

Figure 6. Samples morphology before (a,b) and after (c,d) 1 day and (e,f) 14 days immersion in medium.

3.2. Early cell adhesion

Human MSCs early adhesion and morphology were examined both quantitatively and qualitatively at 2, 4 and 24 hours after seeding. In Figure 7 qualitative representative fluorescent images of hMSCs on BA and CTRTi substrates are reported. Human MSCs exhibit a similar morphology 2 hours after seeding, almost all appearing rounded on both BA and CTRTi substrates (Figure 7A and 7D). At 4 hours, the round morphology progressively shifted toward a more prominent branched shape whatever the substrate (Figure 7B and 7E), while at 24 hours a difference was observed between BA and CTRTi as a function of the different substrate topography. In fact, hMSCs cultured onto the nanostructured surfaces exhibited a well-defined branched shape, while a more spindle and elongated morphology characterized those seeded onto the micro-rough substrate (Figure 7C and 7F).

From a quantitative point of view, different morphometric measures were performed to identify the difference perceived by the cells in substrate topography and understand the role of morphometric measures as a predictive tool of phenotypic lineage commitment. No significant differences were detected between the two substrates in terms of Area (Figure 8A) and Perimeter (Figure 8B), as similar values were obtained at each time point. However, a significant increase was recorded in the spreading area onto both substrates, suggesting the ability of both micro and nano/micro-rough substrates to support an efficient adhesion process. The qualitative observation of cell morphology at 24 hours was confirmed by the aspect ratio parameter (AR) that describes the shape of the cells. More in detail, high values for AR are associated with elongated cells shape, while a decrease in this ratio describes cells with a more polygonal shape. At 24 hours this difference was significant as BA substrate value for AR was 2,56±0,94 in comparison with CTRTi substrate 3,61±0,93 ($p < 0.005$). Other significant differences were detected between the two substrates extensively reported in the Figure 8C. Further discrimination between polygonal and circular shapes could also be obtained adopting the circularity parameter, where 1 represents a perfect circle. The circularity (Figure 8D) and roundness (Figure 8E) parameters, instead, progressively decreased with no significant difference between BA and CTRTI substrates, suggesting the ability of both nano- and microstructures surfaces to support cells adhesion and the subsequent spreading phase. Another significant difference ($p < 0.05$) was detected in the elongation index (Figure 8F) parameter that showed a higher value for the CTRTi in comparison to BA substrate (4,54±0,92 vs 3,52±1,19) further suggesting a probably action of the nanotopography on cells shape.

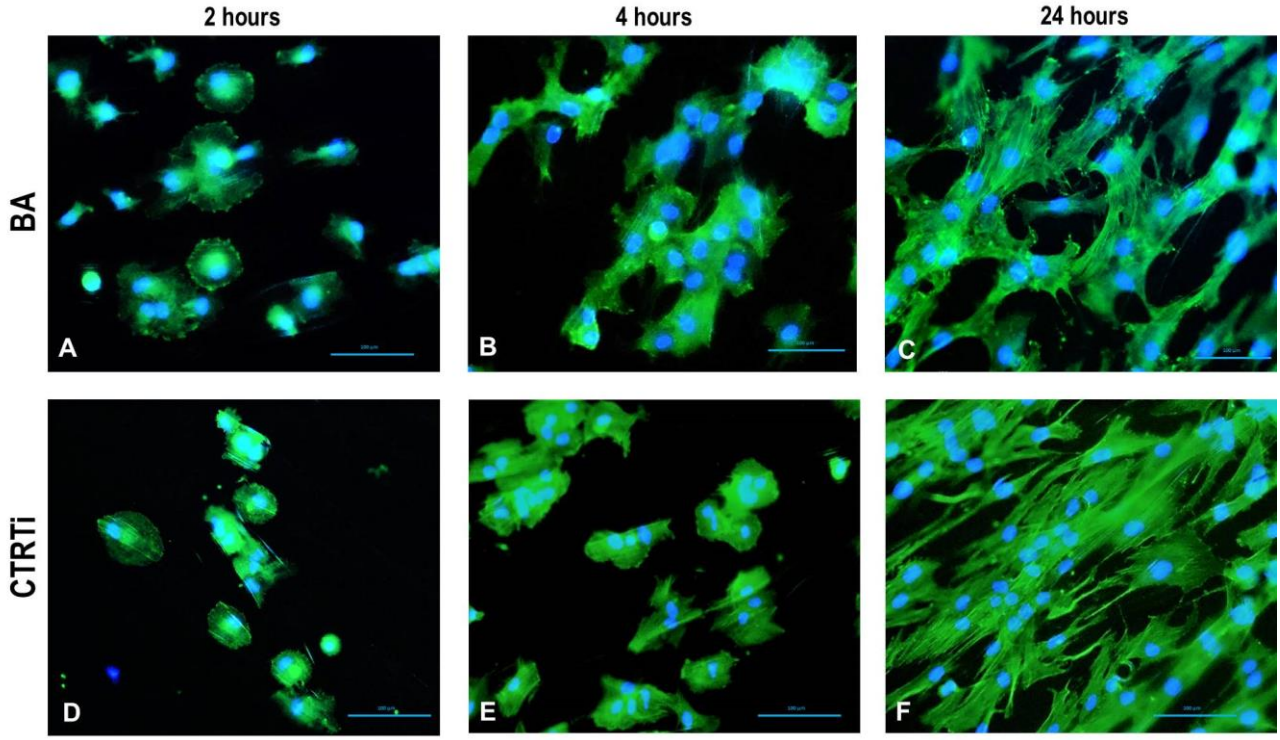

Figure 7. Representative 20X fluorescent images of hMSCs stained with phalloidin (cytoskeleton, green) and DAPI (nucleus, blue) following adhesion onto the biomimetic nanostructured coating (BA substrate: Figure 7A, 7B and 7C) or onto micro-rough titanium control substrate (CTRTi substrate: Figure 7D, 7E and 7F) at 2 (Figure 7A and 7D), 4 (Figure 7B and 7E) and 24 hours (Figure 7C and7). Scale bar indicating 100 um applies to A-F images.

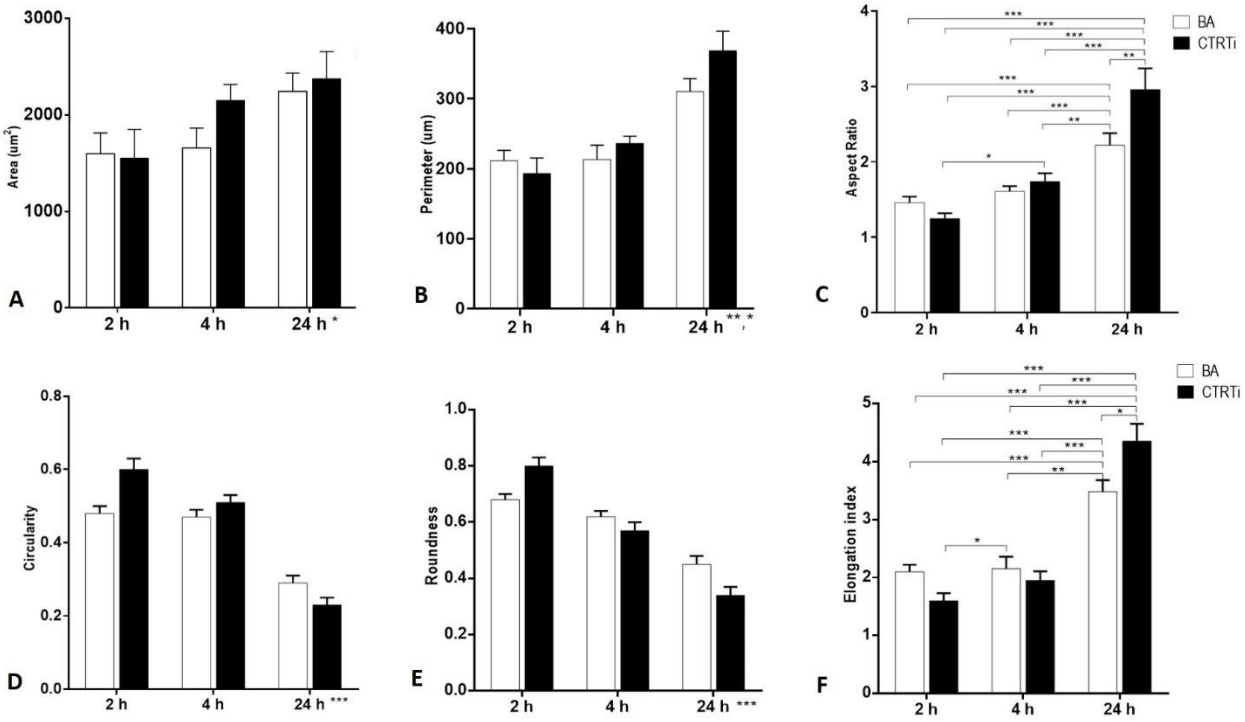

Figure 8. Morphometric descriptors of hMSC shape in response to biomimetic nano/micro structured (BA) and microstrucured topography (CTRTi). Cell shape was quantified in terms of individual cell area (A), perimeter (B), aspect ratio (C), circularity (D), roundness (E) and elongation index (F). Three different fields were acquired for each substrate under investigation at 20x magnification and inside each field at least 10 individual cells were manually outlined. Data are shown as mean ± standard error. (**Area**: *, $p < 0.05$: 24 hours *vs* 2 hours; **Perimeter**: **, $p < 0.0005$: 24 hours *vs* 2 hours and *, $p < 0.05$: 24 hours *vs* 4 hours; **Aspect Ratio**: *, $p < 0.05$; **, $p < 0.005$; ***, $p < 0.0005$; **Circularity:** ***, $p < 0.0005$: 24 hours *vs* 2 hours and 24 hours *vs* 4 hours; **Roundness**: ***, $p < 0.0005$: 24 hours *vs* 2 hours and 24 hours *vs* 4 hours; **Elongation Index**: *, $p < 0.05$; **, $p < 0.005$; ***, $p < 0.0005$).

To deeply characterize the influence of the nanotopography on hMSCs adhesion, at the previously reported experimental times (2, 4 and 24 hours) vinculin fluorescent staining was performed to detect focal adhesion points. Representative images at 24 hours of hMSCs seeded onto BA substrate were reported in Figure 9 to highlight the adhesion of the spreading cells onto the BA substrates, which is suggested by the well-defined actin filaments in green (Figure 9A). The epifluorescent staining detected both the cytoplasmic vinculin and the focal adhesion points located mainly at the edges of the hMSCs. From statistical point of view no significant differences were detected in the number of FA/μm^2 between BA and CTRTi substrate (Figure 9A) while for FA Area (μm^2) a significant difference was detected between BA substrate at 24 hours versus BA at 2 hours ($p < 0.005$) as well as for CTRTi at 24 hours versus 2 hours ($p < 0.005$) (Figure 9B).

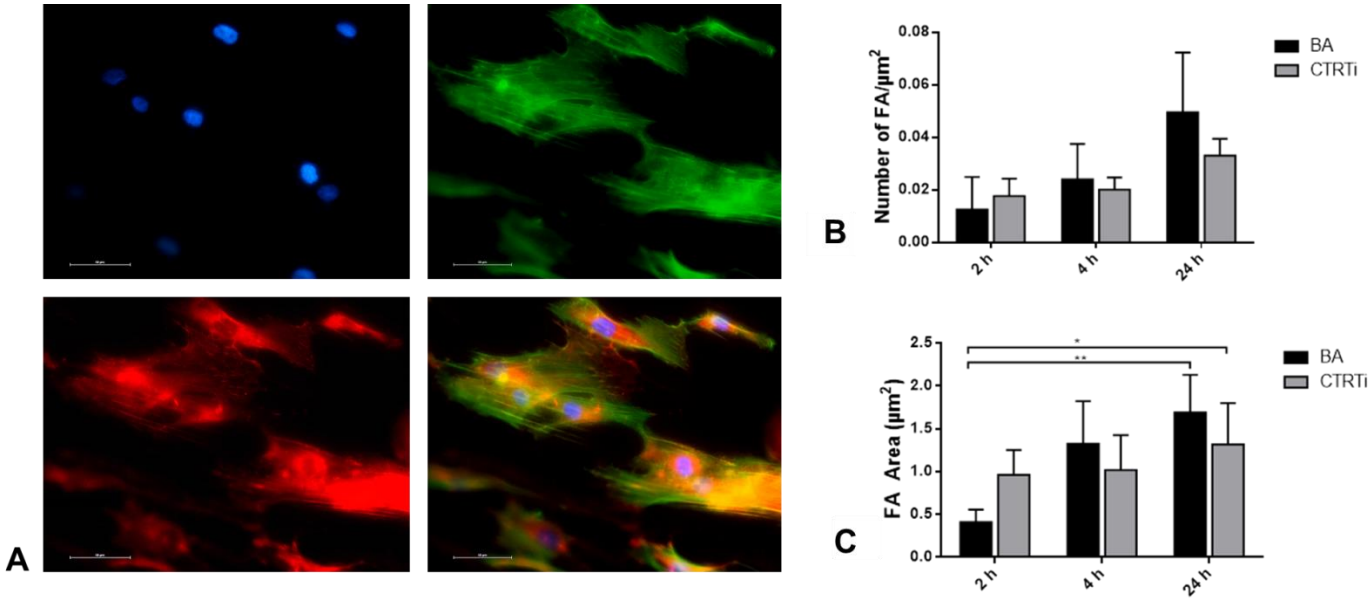

Figure 9. Representative images of hMSCs stained with dapi (nuclear stain, blue), phalloidin (cytoskeleton, green) and vinculin (red). The different staining allowed the direct visualization of F-actin cytoskeleton fibers and the distribution of vinculin at cytoplasmic level as well as focal adhesion points located at the edge of the cells. The three channel images were also merged to visualize the combination of the immunofluorescent stainings Scale bar indicating 50 µm applied to all images (A). Grey boxes reported the quantitative measures of Number of FA/ µm^2 (B) and the measured FA Area (µm^2) for cells seeded onto BA and CTRTi substrates. (**FA Area (µm^2)**: **, $p < 0.005$*:* BA at 24 hours *vs* BA at 2 hours and *, $p < 0.05$*:* CTRTi at 24 hours *vs* BA at 2 hours).

3.3. Scanning electron microscopy

The hMSCs substrates colonization and spreading was visualized by SEM at 3, 7 and 14 days after seeding. At 3 days, the surfaces of all substrates were covered by hMSCs. Onto the nanostructured surfaces a partial delay in the complete substrate covering was observed in comparison to control, as suggested by areas in which the nanosized globular aggregates of the coatings were still visible next to areas completely covered by hMSCs monolayer (Figure 10A, D and G). From 3 to 7 days, the cells proliferate onto each substrate, forming a multilayer that completely cover the surface features (Figure 10B, E, H). At 14 days a complete and complex cells layers formation was visible especially onto nanostructured coatings where the creep, probably occurred during the dehydration process showed stratified cells layers, the presence of many cytoskeletal extensions and an intimate contact among cells (Figure 10C and F). The cells layer onto the control substrate appeared more uniform and flatter (Figure 10I).

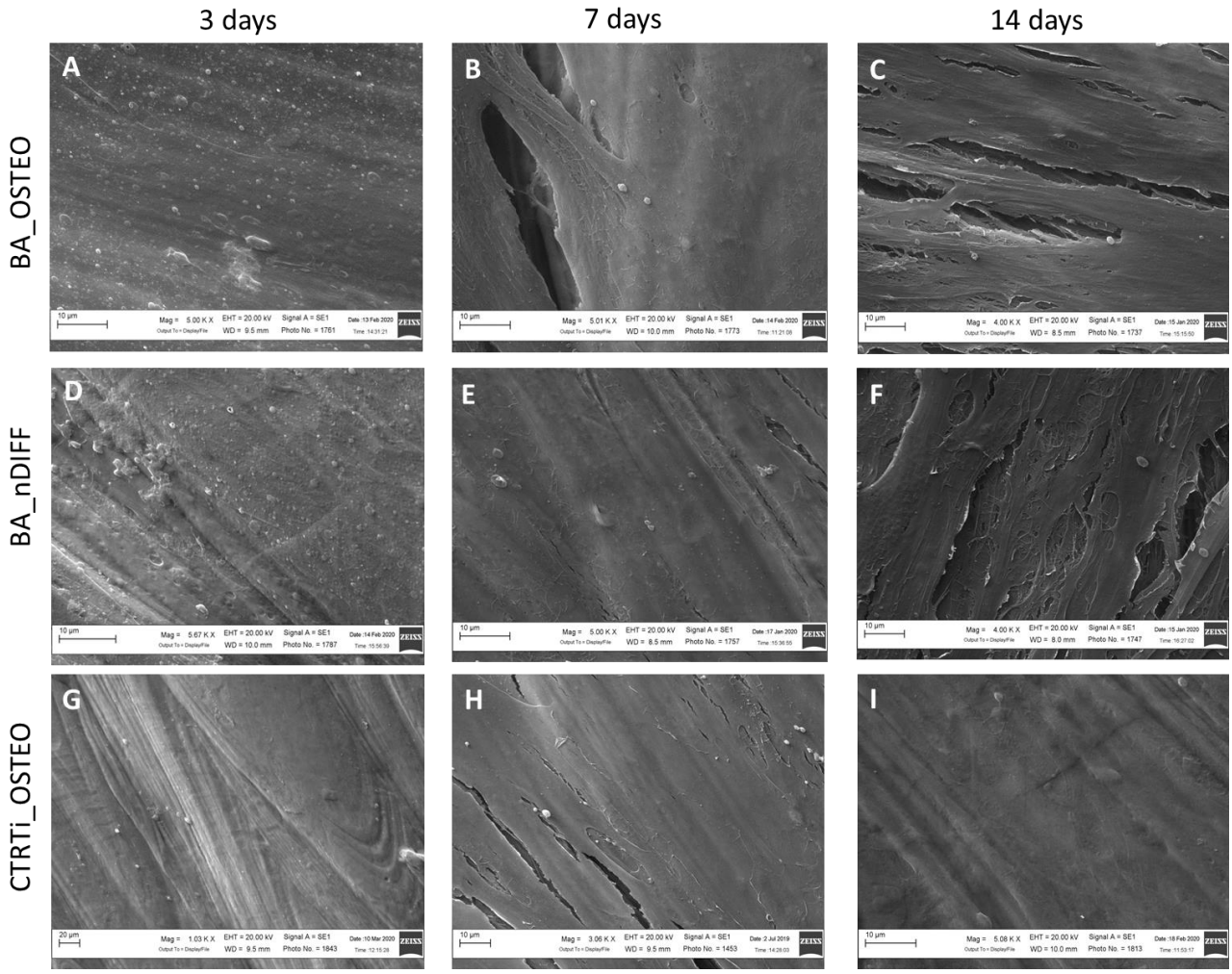

Figure 10. Representative SEM images of hMSC grown onto the different substrates at 3 (Figure 10A, D and G), 7 (Figure 10B, E and H) and 14 days (Figure 10C, F and I) acquired with EVO/MA 10 Zeiss. Figures 10A, B and C refers to the nanostructured biogenic apatite coatings in osteogenic differentiation medium while Figure D, E and F refers to the nanostructured coatings in standard culture medium. Finally, in Figures G, H and I, images of titanium control substrates cultured in osteogenic differentiation medium were reported.

3.4. Cell metabolic activity

In the Alamar Blue test, the absorbance value obtained for resorufin reduction is proportional to the number of viable, metabolically active cells. The absorbance values can be converted to a percentage of reduction of the Alamar Blue: higher percentage of reduction correspond to a higher absorbance value that suggest a greater number of viable cells. In the present *in vitro* set-up, Alamar Blu test (Figure 11), carried out at 3 days, showed a significantly higher metabolic activity for the hMSCs grown on BA in standard medium compared to the cells grown on the same substrate

(BA_nDIFF vs BA_OSTEO: p < 0.005) and on the CTRTi in osteogenic medium (BA_nDIFF vs CTRTi_OSTEO: p < 0.005).

At 7 days, no statistically significant difference was observed between the conditions BA_nDIFF and BA_OSTEO, while the metabolic activity of the CTRTi in osteogenic medium was significantly higher in comparison to both BA conditions at a significance level of p < 0.0005. Even at 14 days, no significant differences were detected between BA_nDIFF and BA_OSTEO, while the metabolic activity of the cells grown onto both substrates was significantly higher than that of the hMSC grown onto CTRTi substrate (BA_nDIFF and BA_OSTEO vs CTRTi_OSTEO: p < 0.005). Therefore, the metabolic activity was in constant growth without significant differences between the condition in osteogenic medium and that in basal medium, thus emphasizing a positive response of the hMSCs to the coating.

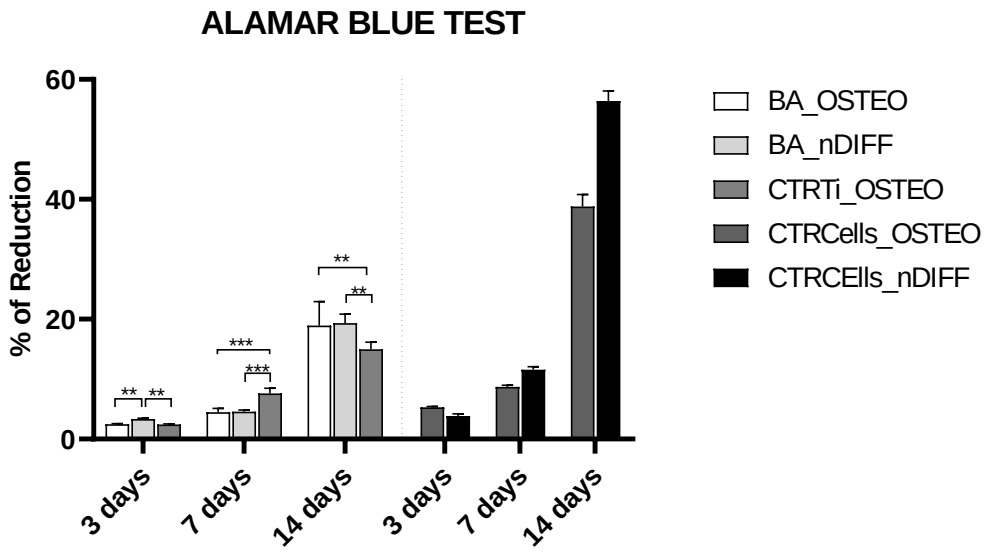

Figure 11: Metabolic activity of h-MSCs seeded onto biogenic apatite nanocoating (BA) in osteogenic (BA_OSTEO) or in standard medium (BA_nDIFF) and onto microrough titanium substrate (adopted as a control substrate) in osteogenic medium (CTRTi_OSTEO) at 3, 7 and 14 day of culture. Bars present the median ± standard deviation obtained from three replicate materials. (*******: p < 0.0005; ******: p < 0.005)

3.5. Gene expression

To verify the hypothesis that the coating micro/nanostructure and biochemical cues can support the osteogenic differentiation of MSCs, their gene expression profile in standard or osteogenic medium was analyzed.

For what regards the genes implicated in the early differentiation towards the osteoblastic phenotype, at 3 days, no significant differences were found between BA_OSTEO and CTRTi_OSTEO in RUNX2, ALPL, SPARC and COL1A1 gene expression, while BMP2 was significantly lower in BA_OSTEO condition in comparison to CTRTi_OSTEO (p <0.005). For all the investigated genes, the BA_nDIFF condition was significantly lower than BA_OSTEO and

CTRTi_OSTEO at different level of significance (see Figure **12**) except for, osteocalcin gene (BGLAP) that was significantly higher in BA_nDIFF condition in comparison to BA_OSTEO and CTRTi_OSTEO cultures (p <0.0005).

At 7 days, the expression of BGLAP was still higher in BA_nDIFF condition in comparison to BA_OSTEO and CTRTi_OSTEO cultures (p <0.0005). Gene expression of RUNX2 was also significantly higher in BA_nDIFF in comparison to BA_OSTEO and CTRTi_OSTEO cultures (p <0.005).

For the genes encoding alkaline phosphatase (ALPL), Type I collagen (COL1A1) and osteonectin (SPARC), the expression was higher in the BA_OSTEO (p <0.0005) and CTRTi_OSTEO (p <0.0005) in comparison to BA_nDIFF. In addition, for ALPL gene, a significance was also detected between BA_OSTEO and CTRTi_OSTEO (BA_OSTEO *vs* CTRTi_OSTEO: p <0.0005), while for SPARC and BMP2 expression the CTRTi_OSTEO condition was significantly higher in comparison to BA_OSTEO (p <0.0005).

The BGLAP level at 14 day for BA_OSTEO was significantly higher in comparison to both BA_nDIFF condition (p <0.0005) and CTRTi (p <0.005). At this timepoint, RUNX2 expression level still remained higher for BA_nDIFF compared to BA_OSTEO (p <0.0005), but not toward CTRTi_OSTEO condition, that showed the highest expression level for this gene (CTRTi_OSTEO *vs* AB_OSTEO: p <0.0005 and CTRTi_OSTEO *vs* AB_nDIFF: p <0.005). A similar trend was also observed for ALPL and COL1A1 gene expression, while for BMP2 a peak of expression for BA_nDIFF was observed at 14 days compared to both BA_OSTEO (p <0.0005) and control condition (BA_nDIFF vs CTRTi_OSTEO; p <0.0005). A significance was also present between CTRTi_OSTEO in comparison to BA_OSTEO (p <0.0005). Also, SPARC gene expression at 14 day in BA_nDIFF condition was significantly higher compared to the other two conditions at the same level of significance. Finally, CTRTi_OSTEO was higher in SPARC expression with respect to BA_OSTEO (p <0.005).

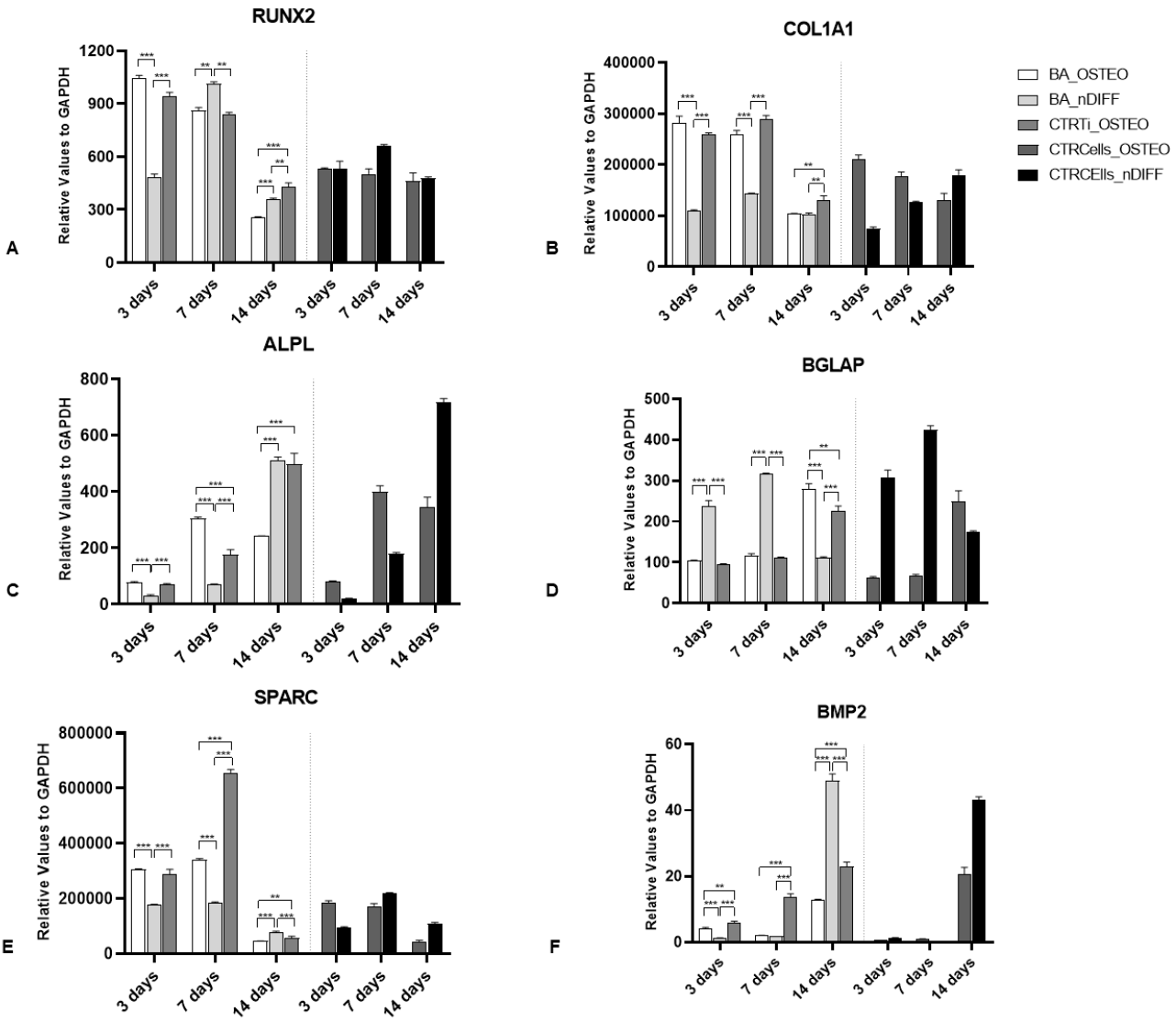

Figure 12. Gene expression of osteogenic markers in different conditions at 3, 7 and 14 day of culture in osteogenic medium (OSTEO) or in standard medium (_nDIFF). The results show the mean ± SE (n = 3). In the graphs, significant differences (******, $p < 0.005$ and *******, $p < 0.0005$) are indicated by bar.

3.6. **Immunoenzymatic Assays**

To further confirm the differentiation process of hMSCs on nanostructured biogenic apatite coating, some osteogenic biomarkers were quantified by the ELISA assay (Figure 13). Osteocalcin and Alkaline Phosphatase represent key protein for the bone formation and mineralization while collagen type I was selected as a good indicator for cell differentiation as it represents one of the major components of bone matrix.

At 3 days no significant differences in the amount of the released osteocalcin or alkaline phosphatase were detected among the different culture conditions, while collagen type I protein detected in the BA_OSTEO condition was significantly higher compared to the other two conditions (BA_OSTEO *vs* BA_nDIFF; p <0.005 and BA_OSTEO *vs*

CTRTi_OSTEO; p <0.05). A significant difference was also present between CTRTi_OSTEO condition versus BA_nDIFF (p <0.05). At 7 days the amount of osteocalcin in BA_nDIFF condition was significantly higher than both BA_OSTEO and CTRTi_OSTEO conditions at the same level of significance (p <0.005) as well as the amount of alkaline phosphatase in the BA_nDIFF condition was higher in comparison to BA_OSTEO condition (p <0.05). No significant differences were detected for collagen biomarker at 7 days among conditions. Finally, at 14 days, an increase in the released proteins amount in the supernatant was observed for all three markers, and a significant osteocalcin production was observed in the BA_nDIFF in comparison to both BA_OSTEO and CTRTi_OSTEO (p <0.0005). Instead, no significant differences were detected for alkaline phosphatase and collagen type I at 14 days.

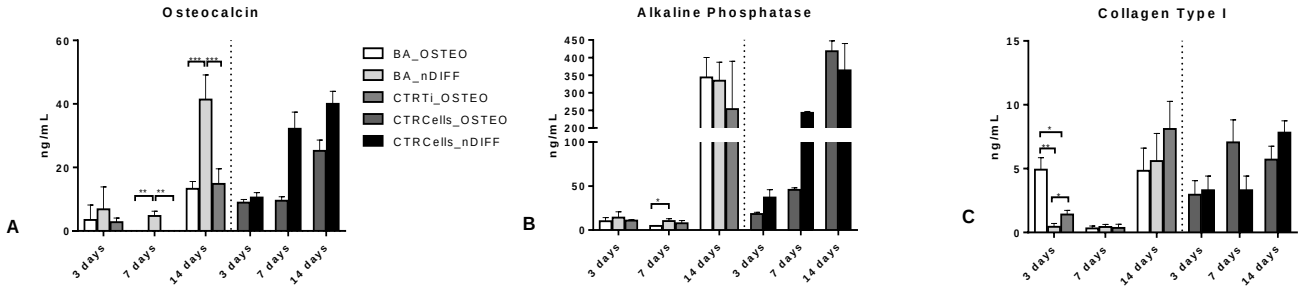

Figure 13. Quantification of bone protein production by hMSCs: (a) osteocalcin, (b) alkaline phosphatase, and (c) collagen type I in the different conditions at 3, 7 and 14 day of culture in osteogenic medium (OSTEO) or in standard medium (_nDIFF). The results show the mean ± SE (n = 3). In the graphs, significant differences (*****, $p < 0.05$ ******, $p < 0.005$ and *******, $p < 0.0005$) are indicated by bar.

4. DISCUSSION

Strong fixation and implant stability represent fundamental cornerstones for osseointegration and the clinical success of implantable devices. In this delicate balance of factors and conditions, the choice of material and its functionalization characteristics are key players. In fact, the material interface can promote osteointegration by acting on early events of adhesion and migration, influencing the differentiation of cells and their ability to colonize the implant surface [38].

In this study, the topographical cues of titanium surface were combined to a biomimetic nanostructured coating and this cues association was challenged with hMSCs. Our findings confirmed the biocompatibility of the biomimetic coating [30]. It is a well-known that surface roughness at the micrometer but also the sub-micrometer scale increases surface area by favoring cells adhesion and osteogenic differentiation [39]. Proper roughness can promote *in vivo* bone

formation, even in the roughness range considered in the present study for the titanium. It is certainly more recent the finding on how the nanostructure is able to direct MSC differentiation [40, 41].

In this scenario, we obtained and characterized biomimetic CaP coatings with bone-like composition and nanostructured morphology.The coatings were deposited onto microrough titanium topography thus creating a nano/micro-rough biomimetic surface able to drive early response of hMSCs. In fact, many of the pursued approaches tend to rely on a single type of stimulus or aspect rather than creating a multifunctional cell-instructive material. In this view, the present research exploits biomimicry not only as biochemical signal provided by the biogenic apatite but also at the topographical level, i.e., presenting to the cells micro/nano features with a magnitude scale comparable to that of important cellular structures [42, 43]. In fact, the films present a multi-scale morphology, as they are composed by aggregates with a diameter ranging from about 100 nm up to over 2 microns, with the majority of them having a diameter of ~110-120 nm. In terms of composition, FT-IR, GI-XRD and EDX data combined indicate that the coatings are composed by a multi-substituted carbonated hydroxyapatite, having a scarce crystallinity. Starting from bovine bone, a non-stoichiometric bone-like apatite can be obtained by IJD, with an elemental composition very close to the natural bone apatite, presenting carbonate-substitutions and trace ions sodium and magnesium. The coatings show high uniformity in both composition and morphology, among different samples and different areas of each sample. In particular sodium and magnesium are evenly distributed in the coating, in percentages within the range of human and animal bone [44]. The presence of ion-substitutions is crucial in biogenic apatite, as each ion modifies the solubility of hydroxyapatite, modifying the type and amount of ions released in the peri-implant environment and, as a consequence, the implant capability to promote host cells adhesion, proliferation and differentiation. In addition, magnesium and sodium also have an important biological role demonstrated both *in vitro* and *in vivo* [45, 46] and also crystallinity can be tuned by post deposition annealing, which permits to determine a suitable dissolution profile [44]. The biomimicry exploited at chemical level was further synergized by the combination with the nanometer scale leading to a nano-CaP grains with higher specific surface, low crystallinity and structural uniformity [47]. The produced micro/nanoscale characteristics of titanium substrate are perceived by hMSCs as they possess the ability to discriminate between the topographic characteristics. The coupling between micro- and nano topography seems to be more effective in promoting cells adhesion and in modulating the differentiation process as these different topographies act on different cellular phases [48]. Therefore, the surface characteristics of the substrate were perceived by hMSCs from a morphological point of view, as this crosstalk with the surface acts especially at the cytoskeleton level by stimulating the contractile activity, which increases intracellular tension and leads to the expression pathway related to the osteoblast phenotype [49, 50]. Even if the study of the focal adhesion points by vinculin staining did not show a significant difference between the microrough control and the nano/micro-rough biomimetic surface, at 24 hours an higher density and a

greater area of focal adhesion points were observed for the hMSCs seeded onto the nanostructured biomimetic coating. Larger focal adhesions suggest a strong interaction with the substrate and an increased mechanotranduction stimulation and cytoskeleton contractility that as aforementioned, could represent favoring factors for the osteogenic commitment of hMSCs [49, 50].

To further quantify "how" and "how much" different environmental factors, such as topography, chemistry, mechanical or biophysical stimuli, can act on cells and their differentiation pathway, the measure of morphometric parameters related to cell morphology represent a raising approach in different fields of investigation [51]. In fact, the qualitative observation and the quantitative data obtained from the early adhesion and morphology evaluation seem to be predictive of the osteogenic differentiation of hMSCs. Here, no significant difference was observed in cell morphology after a few hours from seeding, but at 24 hours, hMSCs seeded onto BA nanostructured surface gained a branched shape, while those seeded on CTRTi microrough substrate exhibited a more elongated morphology. Similar observations have been previously reported by Lavenus et al, when describing the adhesion and differentiation process of MSCs as a function of different nanostructures (30, 150 and 300 nanometer size), obtained by physical vapor deposition suggesting a significant impact of nano-features on osteogenic differentiation, also depending on their size [52].

Cell aspect ratio, circularity and elongation index represent well-established measures of cell morphology and phenotype commitment [53]. As demonstrated by several literature reports, cell shape is linked to cell phenotype and is strongly influenced by the stimuli perceived through the cell-material interactions and by the so-created environment [54]. Here, one hour after seeding, all hMSCs presented a round shape, as suggested by a high circularity parameter and low aspect ratio, while at 24 hours, some differences in cells morphology appeared more evident among the two substrates: a greater elongation and spindle morphology was noticed for hMSCs onto microrough control substrate (CTRTi, confirmed by a 4.54 of elongation index, an aspect ratio of 3.61 and circularity value of 0.27), compared to a more branched morphology (3.52 of elongation index, aspect ratio of 2.56 and circularity value of 0.32) exhibited by cells onto BA coatings. These results agree with data recently reported by Long et al, in which a comparison is presented between macro/micro textured and nano/roughened titanium surfaces. The morphometric values of cells morphology confirmed how the topographic feature of materials are able to influence and direct the differentiation process [55].

Further evaluations (SEM, metabolic activity, differentiation process by gene expression quantification and ELISA assays) were done also considering the seeding and culturing of hMSCs onto biogenic micro/nanostructured surfaces in medium without the addition of osteogenesis-inducing factors (such as dexamethasone, β-glycerophosphate and ascorbate-2-phosphate). Regarding metabolic activity, no differences were detected between the BA substrate in

osteogenic medium and BA in standard medium during the culture, suggesting that the nanostructured surface texturing and the chemical composition sustain the metabolic activity in a similar manner as the osteogenic medium. Regarding the osteogenic differentiation, at 3 days the osteogenic medium stimulated a comparable gene expression between BA_OSTEO and CTRTi_OSTEO, as no significant differences were detected for almost all of the evaluated genes. It is interesting to note that the significant up-regulation of RUNX2 for BA-nDIFF condition was expressed later in comparison to what observed for the other two conditions: a peak of transcript expression was achieved at 7 days in the absence of inducing factors, while for conditions in differentiating medium, RUNX2 values reached the highest values at 3 days and were already decreasing at 7 days. It is well known that RUNX2 is essential for osteogenesis and represent an early indicator of osteoblast differentiation [56]. Hence, this shift of expression probably determines a later up-regulation of the genes directly regulated by RUNX2 as osteocalcin (BGLAP), alkaline phosphatase (ALPL) and bone morphogenetic protein 2 (BMP2), whose peak of transcription was shifted to 14 days. This explains the reason why no significant expression levels for genes related to late osteogenic differentiation were detected in the BA_nDIFF condition, at the experimental time investigated in this study.

In this pattern of expression, a BGLAP gene exhibit a peculiar trend of expression. Osteocalcin (BGLAP) is normally produced by mature osteoblasts during matrix mineralization, thus representing a late marker of differentiation, but it is reported that its up-regulation can also be detected during proliferation in an early phase of osteogenesis [57]. Other factors may have also influenced early osteocalcin expression: i) the presence of the nanostructured CaP coating; ii) the greater availability of ionic species as carbonate, calcium and phosphorus from the biomimetic coating which may acted directly on specific transduction pathways related to BGLAP gene activation, as already observed both for hMSCs and SAOS-2 [58, 59]. A further confirmation of the osteogenic differentiation induced by the nanostructured biomimetic coating, especially in the BA_nDIFF condition, is provided by the synthesis of some key proteins involved in osteogenesis. Normally, establishing a temporal relationship between gene expression and protein secretion is not trivial, as several levels of gene regulation exist. Despite this, gene expression and protein variation for some key proteins detected in the present study (osteocalcin, alkaline phosphatase and collagen type I) seem to be time-related. For example, for Osteocalcin or BGLAP in the BA_nDIFF condition, the high gene transcription level obtained at 3 and 7 days resulted in a significant protein release in supernatants at 14 days. The same trend was also observed for Collagen Type I, where the gene expression at 3 and 7 days resulted in a detectable protein amount at 14 days. A slow but increasing ALPL gene activation at 3 and 7 days for BA_nDIFF with a peak of expression at 14 days, leads to an important protein release already at 14 days (Figure 13).

In summary, all the investigated genes were modulated in their expression by the tested substrates, but the most important aspect was that the BA micro/nanostructured coating is able to support adhesion, proliferation and to trigger a

signaling pathway that promotes the osteogenic differentiation of MSCs, as confirmed by protein quantification of osteocalcin, alkaline phosphatase and collagen type I, even in the absence of specific commitment provided by the osteogenesis-inducing factors [60].

5. CONCLUSION

Topographical and chemical cues represent very active stimuli able to orchestrate the cell phenotype. IJD technique associated with the use of a biomimetic source of CaP is able to produce a nano-sized coating of non-stoichiometric highly substituted bone apatite. This very close compositional and dimensional similarity to the bone inorganic constituent represent a hot spot in bone regenerative approach. All these combined elements lead to a *smart biomaterial* that is able to direct adhesion, to sustain proliferation and to stimulate the expression of key genes and the release of prominent protein for osteogenic commitment and differentiation per se, without the support provided by the inducing factors of the medium.

6. ACKNOWLEDGEMENTS

The research was partially funded by the METACOS Project "Trattamento delle amputazioni mediante osteointegrazione" granted by INAIL-Istituto Nazionale Assicurazione Infortuni sul Lavoro and by Ricerca Corrente provided to Rizzoli Orthopedic Institute.

Gabriela Graziani acknowledges the project Starting Grant SG-2018-12367059, funded by the Italian Ministry of Health (BANDO RICERCA FINALIZZATA 2018).

7. REFERENCES

[1] K. Ong, M. Yun, J. White, New biomaterials for orthopedic implants, Orthop Res Rev. 7 (2015) 107-130.

[2] M. Kaur, K. Singh, Review on titanium and titanium based alloys as biomaterials for orthopaedic applications, Mater Sci Eng C Mater Biol Appl. 102 (2019) 844–862.

[3] E. Boanini, P. Torricelli, F. Sima, E. Axente, M. Fini, I.N. Mihailescu, A. Bigi, Gradient coatings of strontium hydroxyapatite/zinc β-tricalcium phosphate as a tool to modulate osteoblast/osteoclast response, J Inorg Biochem. 183 (2018) 1–8.

[4] Boanini E, Torricelli P, Forte L, S. Pagani, N. Mihailescu, C. Ristoscu, I.N. Mihailescu, A. Bigi, Antiresorption implant coatings based on calcium alendronate and octacalcium phosphate deposited by matrix assisted pulsed laser evaporation. Colloids Surf B Biointerfaces. 2015;136:449–456

[5] X. Liu, M. Li, Y. Zhu, K.W.K. Yeung, P.K. Chu, S. Wu, The modulation of stem cell behaviors by functionalized nanoceramic coatings on Ti-based implants, Bioact Mater. 1(1) (2016) 65–76.

[6] G.M. de Peppo, H. Agheli, C. Karlsson, K. Ekström, H. Brisby, M. Lennerås, S. Gustafsson, P. Sjövall, A. Johansson, E. Olsson, J. Lausmaa, P. Thomsen, S. Petronis, Osteogenic response of human mesenchymal stem cells to well-defined nanoscale topography in vitro, Int J Nanomedicine. 9 (2014) 2499–2515.

[7] Y. Hou, L. Yu, W. Xie, L.C. Camacho, M. Zhang, Z. Chu, Q. Wei, R. Haag, Surface Roughness and Substrate Stiffness Synergize To Drive Cellular Mechanoresponse, Nano Letters 20 (1) (2020)748-757.

[8] A. Andrzejewska, B. Lukomska, M. Janowski, Concise Review: Mesenchymal Stem Cells: From Roots to Boost, Stem Cells. 37(7) (2019) 855–864.

[9] M. Lennerås, K. Ekström, F. Vazirisani, F.A. Shah, K. Junevik, P. Thomsen, O. Omar, Interactions between monocytes, mesenchymal stem cells, and implants evaluated using flow cytometry and gene expression, J Tissue Eng Regen Med. 12(7) (2018)1728–1741.

[10] F. Salamanna, M. Maglio, V. Borsari, G. Giavaresi, N.N. Aldini, M. Fini, Peripheral Blood Mononuclear Cells Spontaneous Osteoclastogenesis: Mechanisms Driving the Process and Clinical Relevance in Skeletal Disease, J Cell Physiol. 231(3) (2016) 521-530.

[11] R.J. Miron, D.D. Bosshardt, OsteoMacs: Key players around bone biomaterials, Biomaterials. 82 (2016)1–19.

[12] J. Pajarinen, T. Lin, E. Gibon, Y. Kohno, M. Maruyama, K. Nathan, L. Lu, Z. Yao, S.B. Goodman, Mesenchymal stem cell-macrophage crosstalk and bone healing. Biomaterials. 196 (2019) 80–89.

[13] F. Veronesi, V. Borsari, M. Sartori, M. Orciani, M. Mattioli-Belmonte, M. Fini, The use of cell conditioned medium for musculoskeletal tissue regeneration. J Cell Physiol. 233(6) (2018) 4423–4442.

[14] R. Takeuchi, W. Katagiri, S. Endo, T. Kobayashi, Exosomes from conditioned media of bone marrow-derived mesenchymal stem cells promote bone regeneration by enhancing angiogenesis. PLoS One, 14(11) (2019) e0225472.

[15] P. Kumar, S. Kandoi, R. Misra, S. Vijayalakshmi, K. Rajagopal, R.S. Verma, The mesenchymal stem cell secretome: A new paradigm towards cell-free therapeutic mode in regenerative medicine, Cytokine Growth Factor Rev. 46 (2019)1–9.

[16] M. Meskinfam, S. Bertoldi, N. Albanese, A. Cerri, M.C. Tanzi, R. Imani, N. Baheiraei, M. Farokhi, S. Farè, Polyurethane foam/nano hydroxyapatite composite as a suitable scaffold for bone tissue regeneration, Mater Sci Eng C Mater Biol Appl. 82 (2018)130-140.

[17] A. Palaveniene, K. Songailiene, O. Baniukaitiene, S. Tamburaci, C. Kimna, F. Tihminlioğlu, J. Liesiene, The effect of biomimetic coating and cuttlebone microparticle reinforcement on the osteoconductive properties of cellulose-based scaffolds, Int J Biol Macromol. 152 (2020)1194-1204.

[18] J.V. Rau, A. Generosi, S. Laureti, V.S. Komlev, D. Ferro, S. Nunziante Cesaro, B. Paci, V. Rossi Albertini, E. Agostinelli, S.M. Barinov, Physicochemical investigation of pulsed laser deposited carbonated hydroxyapatite films on titanium, ACS Appl Mater Interfaces. 1(8) (2009)1813-1820.

[19] A. De Bonis, V. Uskoković, K. Barbaro, I. Fadeeva, M. Curcio, L. Imperatori, R. Teghil, J.V. Rau, Pulsed laser deposition temperature effects on strontium-substituted hydroxyapatite thin films for biomedical implants, Cell Biol Toxicol. 2020 [published online ahead of print]

[20] J.V. Rau, M. Fosca, I.V. Fadeeva, S. Kalay, M. Culha, M.G. Raucci, I. Fasolino, L. Ambrosio, I.V. Antoniac, V. Uskoković, Tricalcium phosphate cement supplemented with boron nitride nanotubes with enhanced biological properties, Mat. Sci. Eng.C Mater 114 (2020) 111044.

[21] L. Duta, F.N. Oktar, G.E. Stan, G. Popescu-Pelina, N. Serbana, C. Luculescu, I.N. Mihailescu, Novel doped hydroxyapatite thin films obtained by pulsed laser deposition, Appl. Surf. Sci. 265 (2013) 41–49.

[22] L. Duta, N. Mihailescu, A.C. Popescu, C.R. Luculescu, I.N. Mihailescu, G.Çetin, O.Gunduz, F.N.Oktar, A.C. Popa, A. Kuncser, C. Besleaga, G.E. Stan, Comparative physical, chemical and biological assessment of simple and titanium-doped ovine dentine-derived hydroxyapatite coatings fabricated by pulsed laser deposition, Appl. Surf. Sci. 413 (2017) 129–139.

[23] N. Mihailescu, G.E. Stan, L. Duta, M.C. Chifiriuc, C. Bleotu, M. Sopronyi, C. Luculescu, F.N. Oktar, I.N. Mihailescu, Structural, compositional, mechanical characterization and biological assessment of bovine-derived hydroxyapatite coatings reinforced with MgF2 or MgO for implants functionalization, Mater Sci Eng C Mater Biol Appl. 59 (2016) 863-874.

[24] L. Duta, N. Serban, F.N. Oktar, I.N. Mihailescu, Biological hydroxyapatite thin films synthesized by pulsed laser deposition, Optoelectron. Adv. Mater. 7 (2013) 1040–1044.

[25] R. Narayanan, S.K. Seshadri, T.Y. Kwon, K.H. Kim, Calcium phosphate-based coatings on titanium and its alloys, J. Biomed. Mater. Res. B Appl. Biomater. 85 (2008) 279-299.

[26] S.V. Dorozhkin, Calcium orthophosphate coatings, films and layers, Prog. Biometeorol. 1 (2012) 1.

[27] G. Graziani, M. Bianchi, E. Sassoni, A. Russo, M. Marcacci. Ion-substituted calcium phosphate coatings deposited by plasma-assisted techniques: A review Mat. Sci. Eng.C Mater 74 (2017) 219-229.

[28] G. Graziani, M. Berni, A. Gambardella, M. De Carolis, M.C. Maltarello, M. Boi, G. Carnevale, M. Bianchi, Fabrication and characterization of biomimetic hydroxyapatite thin films for bone implants by direct ablation of a biogenic source, Mat. Sci. Eng.C Mater 99 (2019) 853-862.

[29] D. Bellucci, M. Bianchi, G. Graziani, A. Gambardella, M. Berni, A. Russo, V. Cannillo, Pulsed Electron Deposition of nanostructured bioactive glass coatings for biomedical applications, Ceram Int, 43(17) (2017) 15862-15867.

[30] M. Bianchi, A. Pisciotta, L. Bertoni, M. Berni, A. Gambardella, A. Visani, A. Russo, A. de Pol, G. Carnevale, Osteogenic Differentiation of hDPSCs on Biogenic Bone Apatite Thin Films, Stem Cells Int. 2017 (2017) 6587384.

[31] C. Vater, P. Kaste, M. Stiehler, Culture media for the differentiation of mesenchymal stromal cells, Acta Biomater. 7 (2011) 463–477.

[32] T.L. Riss, R.A. Moravec, A.L. Niles, et al. Cell Viability Assays. 2013 May 1 [Updated 2016 Jul 1]. In: Markossian S, Sittampalam GS, Grossman A, et al., editors. Assay Guidance Manual [Internet]. Bethesda (MD): Eli Lilly & Company and the National Center for Advancing Translational Sciences; 2004. Available from: https://www.ncbi.nlm.nih.gov/books/NBK144065

[33] D. Bates, M. Maechler, B. Bolker, S. Walker, Fitting Linear Mixed-Effects Models Using lme4. J. Stat. Softw. 67 (2015) 1-48.

[34] S.R. Searle, F.M. Speed, G.A. Milliken, Population marginal means in the linear model: An alternative to least squares means, The American Statistician 34 (1980) 216-221.

[35] J.M. Fernández-Pradas, M.V. García-Cuenca, L. Clèries, G. Sardin, J.L. Morenza, Influence of the interface layer on the adhesion of pulsed laser deposited hydroxyapatite coatings on titanium alloy, Appl Surf Sci, 195 (2002) 31-37.

[36] S. Johnson, M. Haluska, R.J. Narayan, R.L. Snyder, In situ annealing of hydroxyapatite thin films, Mater Sci Eng C, 26 (2006) 1312-1316.

[37] G. Graziani, K. Barbaro, I.V. Fadeeva, D. Ghezzi, M. Fosca, E. Sassoni, G. Vadalà, M. Cappelletti, F. Valle, N. Baldini, J.V. Rau, Ionized jet deposition of antimicrobial and stem cell friendly silver-substituted tricalcium phosphate nanocoatings on titanium alloy, Bioactive Materials, 2021, in press.

[38] M. Morra, G. Giavaresi, M. Sartori, A. Ferrari, A. Parrilli, D. Bollati, R. Rodriguez Y Baena, C. Cassinelli, M. Fini Surface chemistry and effects on bone regeneration of a novel biomimetic synthetic bone filler, J Mater Sci Mater Med. 26(4) (2015) 159.

[39] M.B. Berger, D.J. Cohen, R. Olivares-Navarrete, J.K. Williams, D.L. Cochran, B.D. Boyan, Z. Schwartz, Human osteoblasts exhibit sexual dimorphism in their response to estrogen on microstructured titanium surfaces. Biol Sex Differ. 9(1) (2018) 30.

[40] T. Ozdemir, D.T. Bowers, X. Zhan, D. Ghosh, J.L. Brown, Identification of Key Signaling Pathways Orchestrating Substrate Topography Directed Osteogenic Differentiation Through High-Throughput siRNA Screening, Sci Rep 9 (2019) 1001.

[41] E.G. Long, M. Buluk, M.B. Gallagher, J.M. Schneider, J.L. Brown, Human mesenchymal stem cell morphology, migration, and differentiation on micro and nano-textured titanium, Bioact Mater. 4 (2019) 249–255.

[42] A.S.G. Curtis, C.D.W. Wilkinson, Nanotechniques and approaches in biotechnology, Trends Biotechnol, 19 (2001) 97-101.

[43] M.J. Dalby, D. McCloy, M. Robertson, C.D. Wilkinson, R.O. Oreffo RO, Osteoprogenitor response to defined topographies with nanoscale depths, Biomaterials. 27(8) (2006)1306–1315.

[44] G. Graziani, M. Govoni, L. Vivarelli, M. Boi, M. De Carolis, M. Bianchi, E. Sassoni, M.C. Bignozzi, G. Carnevale, F. Marmi, M.C. Maltarello, D. Dallari, A Comprehensive Microstructural and Compositional Characterization of Allogenic and Xenogenic Bone: Application to Bone Grafts and Nanostructured Biomimetic Coatings, Coatings 10(6) (2020) 522.

[45] E. Boanini, M. Gazzano, A. Bigi, Ionic substitutions in calcium phosphates synthesized at low temperature Acta Biomater. 6 (2010)1882-1894.

[46] G. Barbanti Bròdano, G. Giavaresi, F. Lolli, F. Salamanna, A. Parrilli, L. Martini, C. Griffoni, T. Greggi, E. Arcangeli, D. Pressato, S. Boriani, M. Fini, Biomaterials Versus Autologous Bone Graft in Spinal Fusion: An In Vivo Animal Study, Spine (Phila Pa 1976). 39(11) (2014) E661-E668.

[47] M. Bianchi, A. Gambardella, G. Graziani, F. Liscio, M.C. Maltarello, M. Boi, M. Berni, D. Bellucci, G. Marchiori, F. Valle, A. Russo, M. Marcacci, Plasma-assisted deposition of bone apatite-like thin films from natural apatite. Mater. Lett. 199 (2017) 32–36.

[48] P. Chen, T. Aso, R. Sasaki, M. Ashida, Y. Tsutsumi, H. Doi, T. Hanawa, Adhesion and differentiation behaviors of mesenchymal stem cells on titanium with micrometer and nanometer-scale grid patterns produced by femtosecond laser irradiation. J Biomed Mater Res A. 106(10) (2018) 2735–2743.

[49] T. Ozdemir, L.C. Xu, C. Siedlecki, J.L. Brown, Substrate curvature sensing through Myosin IIa upregulates early osteogenesis, Integr. Biol. 5 (2013)1407–1416.

[50] A. Wilkinson, R.N. Hewitt, L.E. McNamara, D. McCloy, R.M. Dominic Meek, M.J. Dalby, Biomimetic microtopography to enhance osteogenesis in vitro, Acta Biomater. 7(7) (2011) 2919–2925.

[51] M.L. Hart, J.C. Lauer, M. Selig, M. Hanak, B. Walters, B. Rolauffs, Shaping the Cell and the Future: Recent Advancements in Biophysical Aspects Relevant to Regenerative Medicine, J. Funct. Morphol. Kinesiol. 3(1) (2018) 2.

[52] S. Lavenus, M. Berreur, V. Trichet, P. Pilet, G. Louarn, P. Layrolle, Adhesion and osteogenic differentiation of human mesenchymal stem cells on titanium nanopores, Eur Cell Mater. 22 (2011) 84-96.

[53] F. Matsuoka, I. Takeuchi, H. Agata, H. Kagami, H. Shiono, Y. Kiyota, H. Honda, R. Kato, Morphology-based prediction of osteogenic differentiation potential of human mesenchymal stem cells, PLoS One. 8(2) (2013) e55082.

[54] B.L. Banik, T.R. Riley, C.J. Platt, J.L. Brown, Human Mesenchymal Stem Cell Morphology and Migration on Microtextured Titanium, Front Bioeng Biotechnol. 4 (2016) 41.

[55] E.G. Long, M. Buluk, M.B. Gallagher, J.M. Schneider, J.L. Brown, Human mesenchymal stem cell morphology, migration, and differentiation on micro and nano-textured titanium, Bioact Mater. 4 (2019) 249–255.

[56] M. Bruderer, R.G. Richards, M. Alini, M.J. Stoddart, Role and regulation of RUNX2 in osteogenesis, Eur. Cell Mater. 28 (2014) 269–286.

[57] M.L. Zoch, T.L. Clemens, R.C. Riddle, New insights into the biology of osteocalcin, Bone 82 (2016) 42–49.

[58] W. Hatakeyama, M. Taira, N. Chosa, H. Kihara, A. Ishisaki, H. Kondo, Effects of apatite particle size in two apatite/collagen composites on the osteogenic differentiation profile of osteoblastic cells, Int J Mol Med. 32(6) (2013)1255–1261.

[59] Y.R. Shih, Y. Hwang, A. Phadke, H. Kang, N.S. Hwang, E.J. Caro, S. Nguyen, M. Siu, E.A. Theodorakis, N.C. Gianneschi, K.S. Vecchio, S. Chien, O.K. Lee, S. Varghese, Calcium phosphate-bearing matrices induce osteogenic differentiation of stem cells through adenosine signaling, Proc Natl Acad Sci U S A. 111(3) (2014) 990–995.

[60] A.B. Faia-Torres, M. Charnley, T. Goren, S. Guimond-Lischer, M. Rottmar, K. Maniura-Weber, N.D. Spencer, R.L. Reis, M.Textor, N.M. Neve, Osteogenic differentiation of human mesenchymal stem cells in the absence of osteogenic supplements: A surface-roughness gradient study, Acta Biomater. 28 (2015) 64–75.